

AD-A246 423



NAVAL POSTGRADUATE SCHOOL  
Monterey, California

2



DTIC  
ELECTE  
FEB 28 1992  
S B D

THESIS

SENSITIVITY OF SENSORS FOR  
CHARACTERIZING CHAOS

by

Lt. Robert G. Vaughan, USN  
December 1991

Thesis Advisor

Ramesh Kolar

Approved for public release; distribution is unlimited.

92 2 25 181

92-04961



REPORT DOCUMENTATION PAGE				
1a REPORT SECURITY CLASSIFICATION Unclassified		1b RESTRICTIVE MARKINGS		
2a SECURITY CLASSIFICATION AUTHORITY		3 DISTRIBUTION/AVAILABILITY OF REPORT Approved for public release; distribution is unlimited.		
2b DECLASSIFICATION/DOWNGRADING SCHEDULE				
4 PERFORMING ORGANIZATION REPORT NUMBER(S)		5 MONITORING ORGANIZATION REPORT NUMBER(S)		
6a NAME OF PERFORMING ORGANIZATION Naval Postgraduate School	6b OFFICE SYMBOL (If applicable) 67	7a NAME OF MONITORING ORGANIZATION Naval Postgraduate School		
6c ADDRESS (City, State, and ZIP Code) Monterey, CA 93943-5000		7b ADDRESS (City, State, and ZIP Code) Monterey, CA 93943-5000		
8a NAME OF FUNDING/SPONSORING ORGANIZATION	8b OFFICE SYMBOL (If applicable)	9 PROCUREMENT INSTRUMENT IDENTIFICATION NUMBER		
8c ADDRESS (City, State, and ZIP Code)		10. SOURCE OF FUNDING NUMBERS		
		Program Element No	Project No	Task No
				Work Unit Accession Number
11 TITLE (Include Security Classification) SENSITIVITY OF SENSORS FOR CHARACTERIZING CHAOS				
12 PERSONAL AUTHOR(S) Vaughan, Robert G.				
13a TYPE OF REPORT Master's Thesis	13b TIME COVERED From To	14 DATE OF REPORT (year, month, day) December 1991	15 PAGE COUNT 68	
16 SUPPLEMENTARY NOTATION The views expressed in this thesis are those of the author and do not reflect the official policy or position of the Department of Defense or the U.S. Government.				
17 COSATI CODES		18. SUBJECT TERMS (continue on reverse if necessary and identify by block number)		
FIELD	GROUP	SUBGROUP		
		Chaos, Nonlinear dynamics, Strange attractor, Fractal dimension, Lyapunov exponent, Poincare section		
19. ABSTRACT (continue on reverse if necessary and identify by block number)				
<p>Chaos describes a class of motions of a deterministic system whose time history is sensitive to initial conditions. Because of the sensitivity of initial conditions, the response of a dynamical system may result in instabilities. Hence, a study of nonlinear response of structures under the expected frequencies of excitation becomes important. Chaotic behavior, for example, may be found in the vibration of large flexible space structures including trusses, booms, and radio antennas. Methods of quantifying chaos have been applied to flexible beams both analytically and experimentally. This research effort investigates the effects of sensors, strain gages and accelerometers, in studying chaotic motions. A long flexible beam is used to model the chaotic behavior, which is also mathematically modelled as Duffing's equation. Time series are recorded and analyzed using pseudo-phase space, Fourier spectrums, Poincare sections, Lyapunov exponents, and fractal correlation dimensions. Comparison of the two sensors is also performed.</p>				
20 DISTRIBUTION/AVAILABILITY OF ABSTRACT		21. ABSTRACT SECURITY CLASSIFICATION		
<input checked="" type="checkbox"/> UNCLASSIFIED/UNLIMITED <input type="checkbox"/> SAME AS REPORT <input type="checkbox"/> DTIC USERS		Unclassified		
22a NAME OF RESPONSIBLE INDIVIDUAL Ramesh Kolar		22b TELEPHONE (Include Area code) (408) 646-2936	22c OFFICE SYMBOL 67Kj	

Approved for public release; distribution is unlimited.

# SENSITIVITY OF SENSORS FOR CHARACTERIZING CHAOS

by

Robert George Vaughan

Lieutenant, United States Navy  
B.S., United States Naval Academy, 1985

Submitted in partial fulfillment of the requirements for  
the degree of

## MASTER OF SCIENCE IN ASTRONAUTICAL ENGINEERING


from the

NAVAL POSTGRADUATE SCHOOL  
December 1991

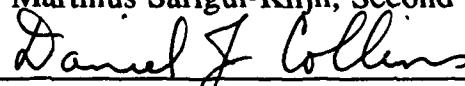
Author:

  
Robert G. Vaughan

Approved by:

  
Ramesh Kolar, Thesis Advisor

  
Martinus Sarigul-Klijn, Second Reader

  
D. Collins, Chairman,  
Department of Aeronautics and Astronautics

## ABSTRACT

Chaos describes a class of motions of a deterministic system whose time history is sensitive to initial conditions. Because of the sensitivity of initial conditions, the response of a dynamical system may result in instabilities. Hence, a study of nonlinear response of structures under the expected frequencies of excitation becomes important. Chaotic behavior, for example, may be found in the vibration response of large flexible space structures including trusses, booms, and radio antennas. Methods of quantifying chaos have been applied to flexible beams both analytically and experimentally. This research effort investigates the effects of sensors, strain gages and accelerometers, in studying chaotic motions. A long flexible beam is used to model the chaotic behavior, which is also mathematically modeled as Duffing's Equation. Time histories are recorded and analyzed using pseudo-phase space, Fourier spectrums, Poincare sections, Lyapunov exponents and fractal correlation dimensions. Comparison of the two sensors is also performed.



Accession For	
NTIS GRA&I	<input checked="checked" type="checkbox"/>
DTIC TAB	<input type="checkbox"/>
Unannounced	<input type="checkbox"/>
Justification	
By	
Distribution/	
Availability Codes	
Dist	Avail and/or Special
A-1	

## TABLE OF CONTENTS

I.	INTRODUCTION .....	1
A.	REASON FOR ANALYSIS .....	1
B.	SCOPE OF THESIS .....	2
II.	THE SCIENCE OF CHAOS .....	3
A.	BACKGROUND AND PREVIOUS STUDIES.....	3
B.	GEOMETRIC AND TOPOLOGICAL METHODS OF CHAOS.....	4
1.	Time Domain Analysis .....	5
2.	Frequency Domain Analysis .....	6
3.	Phase Plane.....	6
4.	Poincare Section.....	8
5.	Lyapunov Exponent .....	9
6.	Fractal Correlation Dimension.....	10
III.	THEORETICAL ANALYSIS .....	19
A.	DUFFING'S EQUATION.....	19
B.	ASSUMED MODES METHOD.....	20
1.	Mass Coefficient Determination .....	22
2.	Stiffness Coefficients Determination .....	23
3.	Damping Coefficient Determination .....	26
C.	THEORETICAL RESULTS.....	28
IV.	EXPERIMENTAL ANALYSIS .....	37
A.	EXPERIMENTAL SET-UP .....	37
B.	EXPERIMENTAL PROCEDURE.....	37
C.	EXPERIMENTAL RESULTS.....	38

V. CONCLUSIONS AND SCOPE FOR FUTURE RESEARCH .....	54
APPENDIX A.....	55
APPENDIX B.....	58
LIST OF REFERENCES.....	59
INITIAL DISTRIBUTION LIST.....	61

## **ACKNOWLEDGEMENTS**

I would like to thank Tom Christian and Jim Scofield of the Mechanical Engineering Department. The experimental portion of this thesis would not have been accomplished without their support. Dan Sakoda of the Space Systems Academic Group also provided much help in the setup of the experiment. I would also like to thank Professor Kolar for his direction and guidance in the completion of this task.

Most importantly, I would like to thank my wife, Cary, who typed this thesis and provided immeasurable encouragement and support.

## **I. INTRODUCTION**

### **A. REASON FOR ANALYSIS**

Many of the satellites currently being launched have highly flexible components such as trusses and booms. Long, highly flexible booms and trusses are used for gravity gradient stabilization, supporting large solar arrays and radio antennas, and ensuring that humans and equipment are adequately shielded from radioactive power generators in some proposed interplanetary spacecraft. Deploying these trusses and booms and maneuvering the satellite for attitude control and station keeping result in large displacements and rotations of the tips. This leads to the presence of geometric nonlinearities in the structure. Material nonlinearities are not usually present since the booms and trusses are not deflected past their yield point and thus the linear stress-strain law applies. Because of the geometric nonlinearities, it is appropriate to model flexible space structures by nonlinear equations of motions instead of linear ones. Duffing's Equation is one equation used to adequately describe the nonlinear behavior due to the elastic effects of these large structures.

The presence of nonlinearities may result in motions which are impossible to predict after long periods of time, yet completely deterministic since the equations of motions are known. Slight changes in initial conditions produce radically different outputs. These types of responses have been characterized as "chaotic." Chaotic vibrations of spacecraft structures could result in control problems.



## B. SCOPE OF THESIS

The purpose of this theses is to demonstrate that chaotic vibrations can occur in highly flexible space structures using theoretical and experimental analyses. For the theoretical analysis, a flexible sheet of aluminum 7 ft. long, 3 in. wide, and 0.080 in. thick, was modelled by Duffing's Equations. This process is described in Chapter III. For the experimental analysis, the same beam was instrumented with strain gauges and accelerometers. The beam was then shaken by an MB Dynamics Model PM500A Vibration Exciter and the time histories of the strains and accelerations were recorded. This process is discussed in Chapter IV. Data from both analyses were then analyzed using the computer program, "Chaos," developed by CDR Martinus Sarigul-Klijn, USN, [Ref. 1].

In addition, the purpose of this thesis is to investigate the sensitivity of sensors in detecting chaotic vibrations. The two most commonly used types of sensors are accelerometers and strain gauges. Measuring accelerations may be a more accurate method of recording the time histories of chaotic systems since this includes inertia, damping, and stiffness terms of the mathematical equations used to model the system. Strain gauges permit measurement of only the stiffness terms of the mathematical equations used to model the system. After a discussion of the Science of Chaos (Chapter II) the results of the theoretical and experimental analyses will be discussed.

## **II. THE SCIENCE OF CHAOS**

### **A. BACKGROUND AND PREVIOUS STUDIES**

A deterministic system whose time history has a sensitive dependence on initial conditions is one definition of a chaotic system [Ref. 2: p. 4]. Even though the equations of motions which adequately describe a system are well known, small changes in the initial conditions produce markedly different outputs. For example, although there are many computer programs which can accurately predict the weather tomorrow, there are no programs which can accurately predict the weather for a day next year. Recognizing that chaos occurs in the nonlinear deterministic models raises the hope of understanding the source of this random-like behavior and possibly doing something to change it.

Although Henri Poincare observed chaotic behavior in the trajectories of some celestial bodies at the beginning of the twentieth century, the science of chaos is a relatively new field. It is one which essentially became possible after the birth of the computer which not only allowed numerical integration of systems of mathematical equations, but also shorter and shorter time intervals at which experimental data could be obtained. In the 1960's Edward Lorenz of MIT used a computer to numerically integrate twelve differential equations which described a crude model of the weather. In his simulations he found dramatic differences in output for subtle changes in input. [Ref. 3: p. 51] Since then, many other researchers have used computers to investigate chaotic behavior in virtually every field including mathematics, biology, chemistry, ecology, economics, physics, medicine, meteorology, and engineering. James

Gleick presents an interesting and easy-to-read development of the science of chaos in *Chaos: Making a New Science* [Ref. 4].

The chaotic behavior of flexible space structures has been studied by Moon and Li. In their analysis of a 3.5 meter long 3-D truss, they found that the free-play in the joints of the structure resulted in chaotic motion and modal frequencies considerably lower than those determined by linear methods. Chaotic dynamics in this structure and other space structures might make it difficult to design active controls to damp out transient dynamics. [Ref. 5] In addition, chaotic dynamics leads to inaccuracies in linear finite element models which are currently used to obtain modal analysis during the design of spacecraft. The results of the Low Power Atmospheric Compensation Experiment (LACE) may lead to improvements of these finite element models. [Ref. 6]

In another study by Moon and Shaw, chaotic vibration were observed in an elastic beam with non-linear boundary conditions. For certain values of forcing frequency and amplitude, the periodic motion became unstable and nonperiodic. The results were typical of a class of mechanical oscillators with play or amplitude constraining stops. [Ref. 7]

## **B. GEOMETRIC AND TOPOLOGICAL METHODS OF CHAOS**

The purpose of this section is to describe several methods which have been developed for detecting chaotic behavior in dynamical systems. The methods which are discussed are time series, phase plane, frequency domain, Poincare section, Lyapunov exponent, and fractal correlation dimension. The first four methods are more qualitative in nature, and answer the question: Is chaos present? The last two methods, Lyapunov exponent and fractal correlation

dimension, are more quantitative in nature. Generally, when determining if chaos is present in a system, several of the above methods are used since applying one method by itself is not always indicative of chaotic motion.

### 1. Time Domain Analysis

The traditional way of observing signals is to view them in the time domain. This is simply a record of what is happening to a parameter of the system versus time. Sometimes the first indication of chaotic motion is that the parameter observed exhibits no pattern or periodicity. This test is not always conclusive, since the motion observed could have a long period behavior that is not readily observable. In addition, some nonlinear systems may appear non periodic, but can be broken down into several periodic signals. [Ref. 2: p. 42]

Figure 2.1 illustrates both the nonperiodic nature of chaotic signals and also the sensitive dependence on initial conditions. Thompson and Stewart numerically integrated the Duffing's equation

$$\ddot{x} + 0.05\dot{x} + x^3 = 7.5 \cos t \quad (2.1)$$

to produce the time history in the figure. The ragged appearance persists for as long a time as the integrations are carried out. There is never an exact repetition of any part of the signal--it is truly nonperiodic. The figure also illustrates that for slight changes in initial conditions, the trajectories quickly diverge. [Ref. 8: p. 4]

## 2. Frequency Domain Analysis

Because of the problems encountered when trying to detect chaos from the time domain, the frequency domain, or Fourier Spectrum, is primarily used. Observing the signal in the frequency domain will instantly reveal if the signal is made up of a sum of periodic signals. Chaotic vibrations will exhibit a broad spectrum of frequencies in the output when the input is a single frequency harmonic motion. Subharmonics and Superharmonics of this frequency will appear not as sharp spikes like the excitation frequency but as rounded hills. Once again, this test is not always conclusive since multiharmonic outputs may result from hidden degrees of freedom of which the observer is unaware. In order to detect chaotic vibrations in large degree-of-freedom systems, it is necessary to observe changes in the spectrum while one parameter such as driving amplitude or frequency is varied [Ref. 2: p. 47].

Figures 2.2 and 2.3 show the Fourier spectrum for a periodic signal generated by the equation

$$\ddot{x} = 3 \cos(4\pi t) \quad (2.2)$$

and the chaotic signal of Equation (2.1) respectively. Notice that Figure 2.2 has a sharp spike only at the excitation frequency while Figure 2.3 has multiple, broadband spikes at frequencies other than the excitation frequency of 0.16 Hz.

## 3. Phase Plane

A dynamical system consists of two parts: the state (essential information about a system) and the dynamic (rule that describes how the state evolves with time). The motion of the system can be visualized in a state space

or phase plane. The phase plane is a construct whose coordinates are components of the state. The coordinates, therefore, depend on the type of system being studied. A mechanical system will usually use position versus velocity. A simple example to describe this is the motion of a pendulum. All that is needed to determine its motion are position and velocity. The state is thus a point on the phase plane. Newton's Laws provide the dynamic, expressed mathematically as a differential equation, that describes how the state evolves. Without the presence of friction, the pendulum traces out a circle or orbit in the phase plane. When friction is present, the orbit spirals in to a single point or attractor. [Ref. 3: p. 49] This describes the motion of a simple non chaotic system. The orbits of chaotic systems never close or retrace themselves. Thus, the trajectory of the orbits will tend to fill up a section of the phase plane. Once again, this is not always a conclusive test for chaos.

The pseudo-phase plane is another technique which has been used when only one variable is able to be measured. This technique was discovered by scientists at the University of Santa Cruz while analyzing a dripping faucet. They constructed a pseudo-phase plane using a measured variable and a time-shifted version of the same measured variable. Takens later proved that a pseudo-phase plane exhibited the same characteristics as a phase plane. [Ref. 4: p. 266] The choice of the time shift or embedding time will shrink or expand the orbit about the line  $y = x$ . Dvorak and Klaschka have proven that an embedding time between five and eleven time intervals produces a pseudo-phase plane with the least amount of bias [Ref. 9]. Chaotic motions exhibits the same characteristics in the pseudo-phase plane as they do in the phase plane.

The pseudo-phase plane for the periodic signal appears as a circle as expected (Figure 2.4). This signal constantly retraces itself. As seen in Figure 2.5, the pseudo-phase plane for the chaotic signal of Equation (2.1) never retraces itself and fills up a section of the plane.

#### **4. Poincare Section**

The Poincare section is constructed by passing a two-dimensional surface through a three-dimensional phase space and observing where the points of the trajectory intersect the plane. This slice can be made through an infinite number of locations to reveal the internal structure of the trajectory. Periodic signals, such as an undamped pendulum, have one point on the Poincare section while signals with multiple harmonics produce a finite number of points on the Poincare section. If the Poincare section does not consist of a finite set of points or a closed orbit, the motion may be chaotic. In undamped or slightly damped chaotic systems, the Poincare section appears as a cloud of unorganized points. In damped chaotic systems, the Poincare section appears as an infinite set of highly organized points which look like parallel lines. If after several enlargements the structure continues to exist, the system is described as having a strange attractor. This embedding of structure within structure is referred to as a Cantor set after the mathematician George Cantor (1845 - 1918). [Ref. 2: p. 52]

Figure 2.6 is the Poincare section of the periodic signal. Notice that there is only one point in the top right hand corner. The damped, chaotic signal, however, appears as a set of points forming parallel lines as shown in Figure 2.7. If this figure were enlarged, the same pattern would emerge after each enlargement. This is referred to as the self-similar property.

## 5. Lyapunov Exponent

The Lyapunov exponent is a measure of the average rate of divergence of trajectories initially separated by an infinitesimal amount. A system is chaotic if it has one or more positive Lyapunov exponents, which means nearby trajectories are diverging [Ref. 10: p. 323]. Lyapunov exponents have proven to be a useful dynamical test for chaotic systems. Since nearby trajectories correspond to nearly identical states, exponential divergence between the trajectories means that predictability of the system is rapidly lost. Systems with subtle, unresolvable initial differences quickly behave differently. [Ref. 11: p. 285] The Lyapunov exponent,  $\lambda$ , is defined as

$$d(t) = d 2^{\lambda t} \quad (2.3)$$

or

$$\lambda = \frac{1}{t} \log_2 \left( \frac{d(t)}{d} \right) \quad (2.4)$$

where :  $d$  is the initial distance between the two trajectories

$d(t)$  is the distance at a later time,  $t$

As indicated in Equation (2.4) a positive exponent means that ' $d(t)$ ' is greater than ' $d$ ' and the trajectories are diverging. A zero exponent indicates ' $d(t)$ ' and ' $d$ ' are the same and the trajectories coincide. A negative exponent indicates ' $d(t)$ ' is less than ' $d$ ' and the trajectories are converging.

A system with  $n$  degrees of freedom has a set of  $n$  exponents, called the Lyapunov spectrum. This spectrum characterizes the divergence of the trajectory in  $n$  directions. In order to understand the meaning of the Lyapunov spectrum, imagine a sphere of neighboring points in the phase space about a



central point on the trajectory. As the points evolve with time, this sphere will deform. If one axis is diverging exponentially the sphere stretches along that direction. If another axis is converging, the sphere shrinks along that direction. Algorithms are available to calculate the exponents of the spectrum from the measurement of a single observed state by constructing the pseudo-phase space. [Ref 12: p. 89] The program "Chaos" uses a method developed by Wolf et al [Ref. 11].

## 6. Fractal Correlation Dimension

The fractal correlation dimension is defined as

$$C(r) \approx r^d \quad (2.5)$$

where:  $C(r)$  is the probability that a point on the attractor is within a  
circle, sphere, or hypersphere of radius ' $r$ '  
 $r$  is the radius of the circle, sphere, or hypersphere  
 $d$  is the fractal correlation dimension.

Solving for ' $d$ ' in Equation (2.5) yields

$$d = \lim \left\{ \frac{\ln[C(r)]}{\ln(r)} \right\} \quad (2.6)$$

$C(r)$  may be calculated by constructing a sphere at each point on the trajectory and counting the number of points in each sphere, such that

$$C(r) = \lim \frac{1}{N^2} \sum_i^N \sum_j^N H(r - |x_i - x_j|) \quad (2.7)$$

where:  $H(s)$  is the Heaviside function and is equal to one if 's' is greater than zero and equal to zero if 's' is less than zero  
 $|x_i - x_j|$  is the Euclidean distance between points  
 $N$  is the total number of points [Ref. 2: p.217]

The procedure used in the "Chaos" program by Sarigul-Klijn to compute the fractal correlation dimension is described below.

1. Start with a point on the attractor and calculate the number of points inside a circle of radius,  $r$ .
2. Calculate the probability  $C(r)$  by dividing this number of points by the total number of points in the attractor.
3. Repeat this for several points along the attractor.
4. Compute  $C(r)$  for several values of  $r$ .
5. The slope of  $\log[C(r)]$  versus  $\log(r)$  yields  $d$ , the fractal correlation dimension, for the chosen number of pseudo-phase space dimensions. [Ref. 1: p. 88].
6. Repeat steps 1 through 5 for higher pseudo-phase space dimensions to obtain an asymptotic estimate of the fractal correlation dimension for the dynamical system.

Nonchaotic systems have integer fractal correlation dimensions such as an equilibrium point (zero), limit cycle (one), or toroidal attractor (two). The fractal correlation dimension of a chaotic system is non-integer and is independent of the dimension of the phase space used for the calculation. [Ref. 13: p. 101]

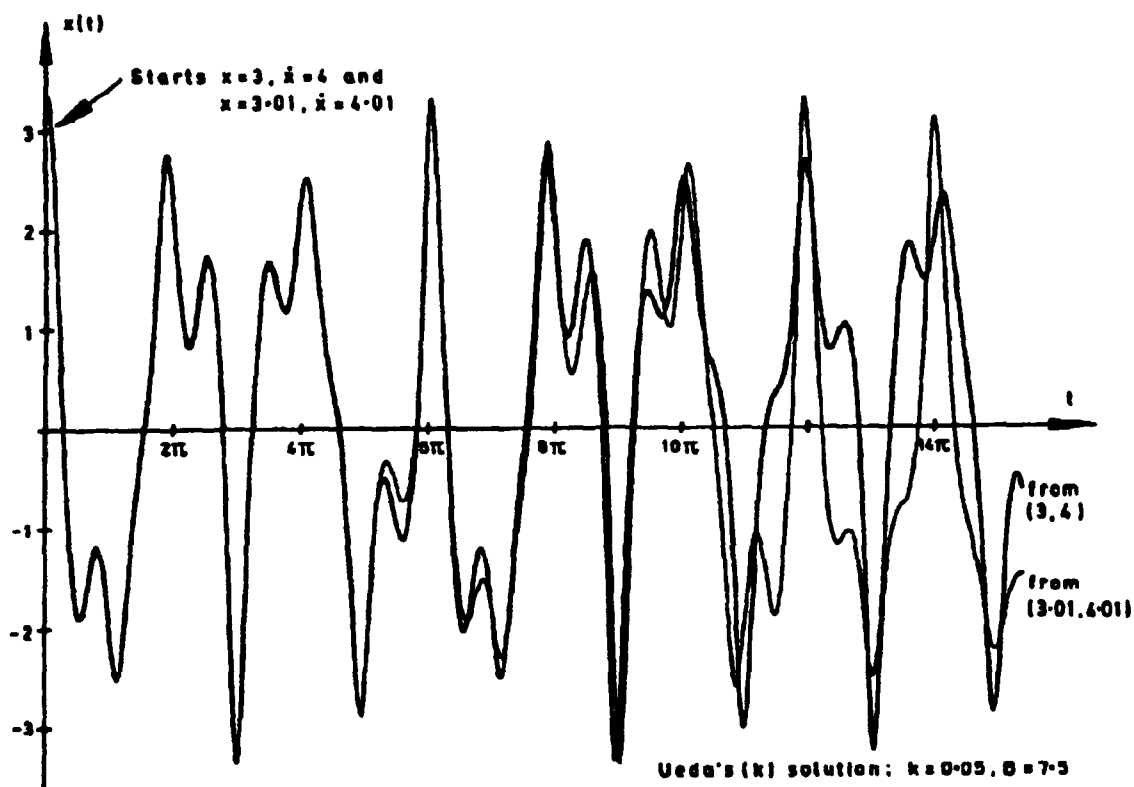
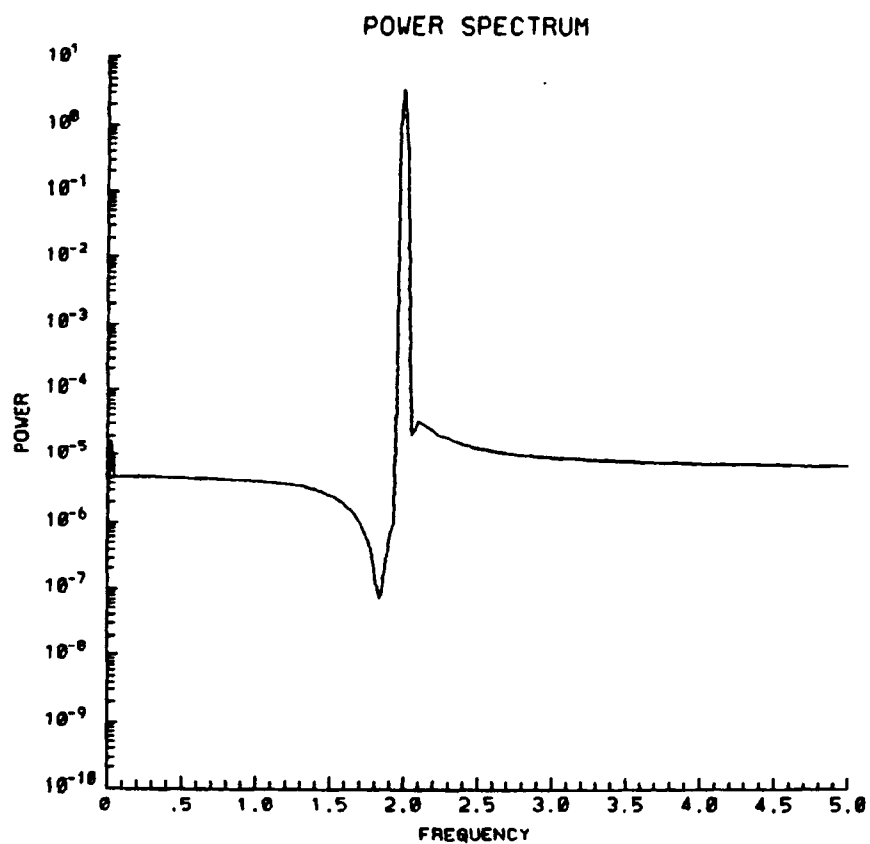


Figure 2.1 Divergence from adjacent starts.



**Figure 2.2 Fourier spectrum of a periodic signal.**

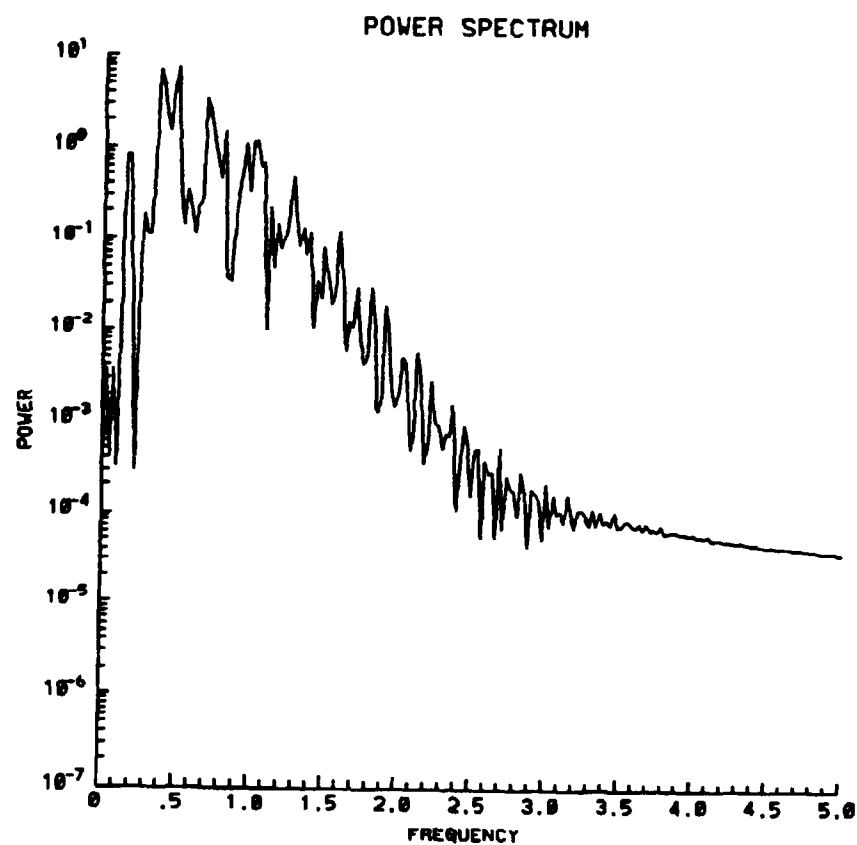
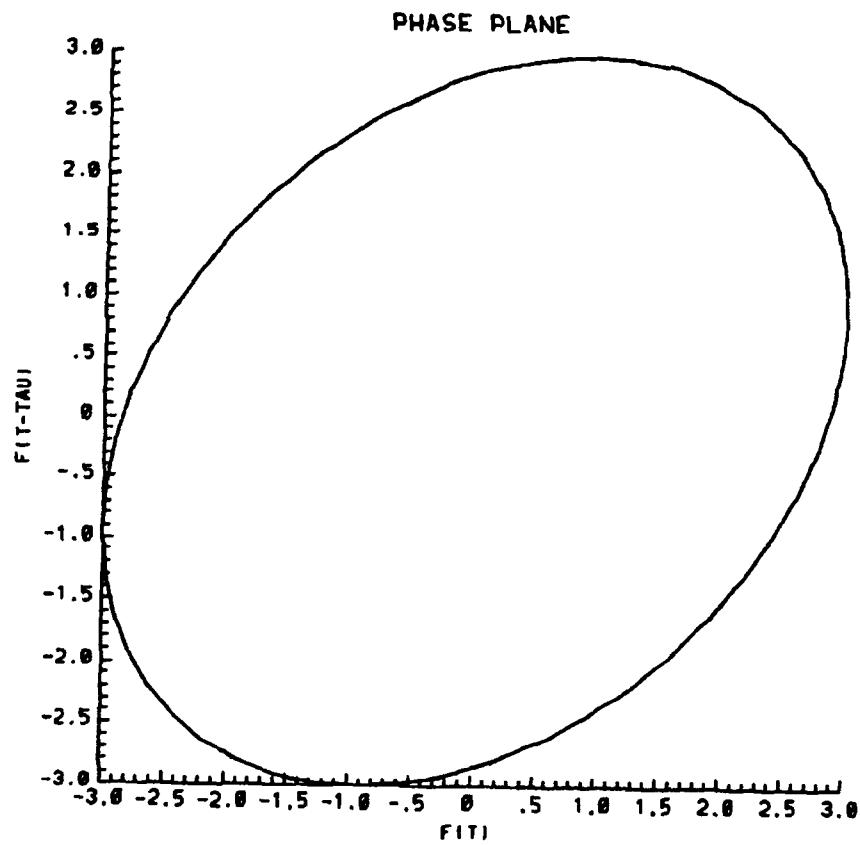
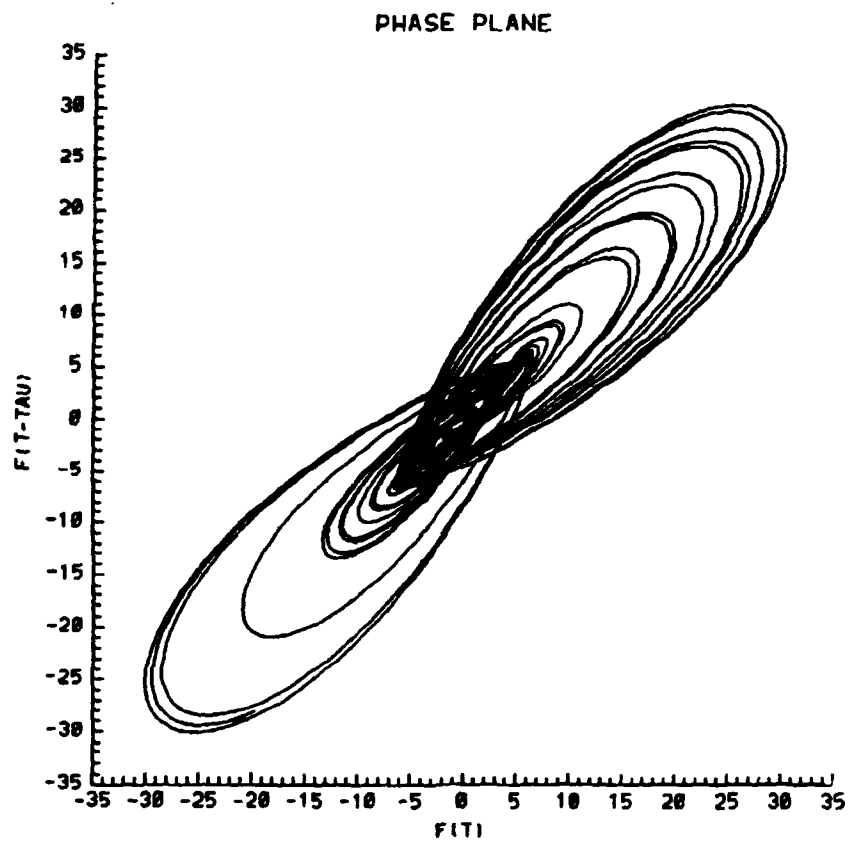


Figure 2.3 Fourier spectrum of a chaotic signal.



**Figure 2.4 Pseudo-phase plane of a periodic signal.**



**Figure 2.5 Pseudo-phase plane of a chaotic signal.**

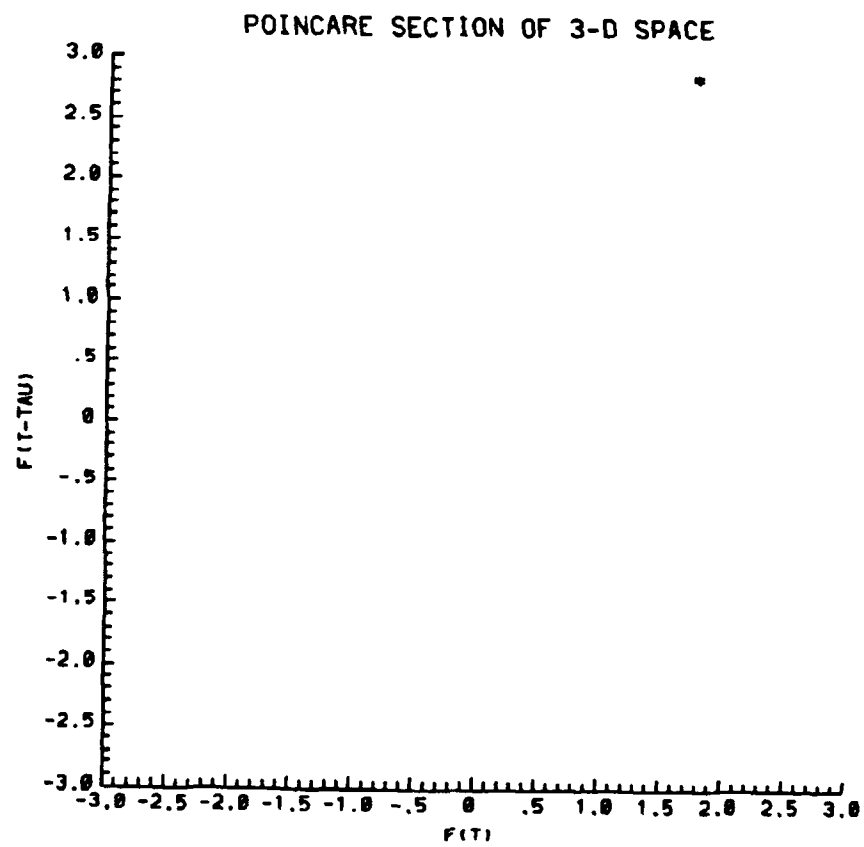
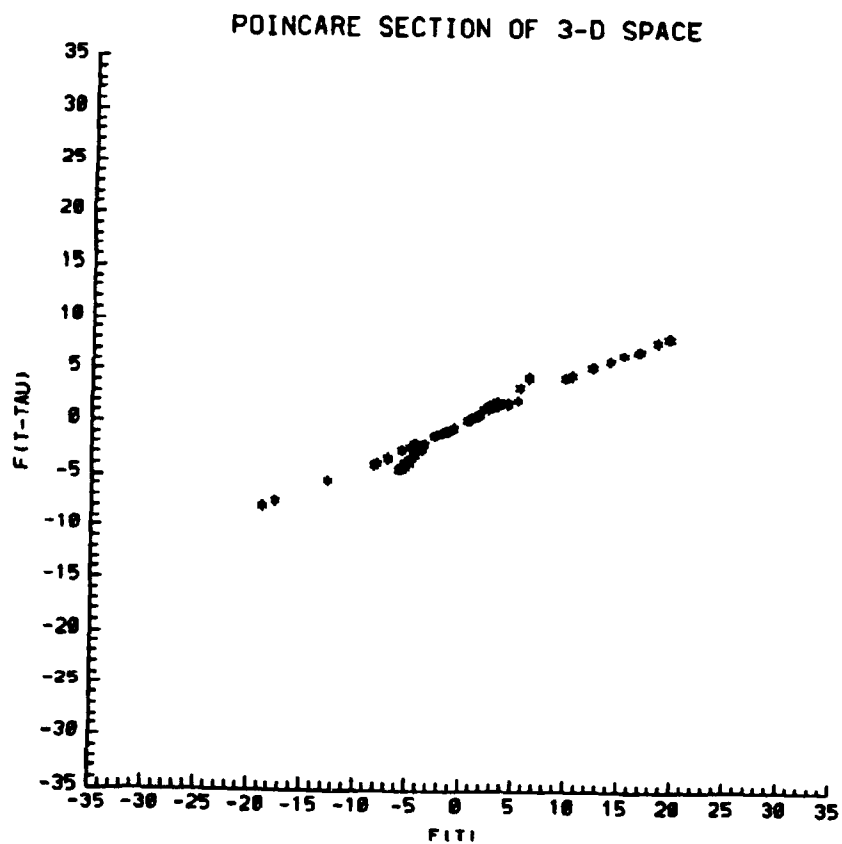


Figure 2.6 Poincaré section of a periodic signal.





**Figure 2.7** Poincare section of a chaotic signal.

### III. THEORETICAL ANALYSIS

#### A. DUFFING'S EQUATION

The mathematical equation which describes the motion of a nonlinear elastic beam is represented by the well-known Duffing's equation.

$$m\ddot{v} + c\dot{v} + k_1v + k_3v^3 = A\cos \omega t \quad (3.1)$$

where:

- $m$  = mass of the beam
- $c$  = damping coefficient
- $k_1$  = linear stiffness coefficient
- $k_3$  = nonlinear stiffness coefficient
- $A$  = amplitude of the excitation
- $\omega$  = frequency of the excitation
- $v$  = transverse displacement of the beam

Once the coefficients of the Duffing's equation are known it can be integrated numerically to solve for the displacement, velocity and acceleration of the tip of a cantilever beam. A fourth order Runge-Kutta scheme (see Appendix A) was developed to perform the integration. The following methods are used to determine the coefficients using the properties of a beam made of 7075-76 sheet aluminum listed in Table 3.1.

## B. ASSUMED MODES METHOD

In order to determine the coefficients to be used in Duffings equation, the assumed modes method is used. This method is an extension of the principle of virtual displacements and is used to produce a generalized parameter model that approximates the flexible behavior of the beam. A virtual displacement is an infinitesimal, imaginary change in the displacement of a system as shown in Figure 3.1.

The dotted curve in the figure shows the virtual displacement,  $\delta v(x,t)$ , of the beam. It must satisfy the same boundary conditions as the actual displacement,  $v(x,t)$ --the solid curve in Figure 3.1. The virtual displacement is not a function of time in the same sense as the actual displacement but is rather a small change of configuration relative to the configuration of the beam at the time "t" [Ref. 14: p. 33].

To create the single degree of freedom model, the deflection of the beam may be approximated by

$$v(x,t) = \psi(x) \vartheta(t) \quad (3.2)$$

Similarly, the virtual displacement is given by

$$\delta v(x,t) = \psi(x) \delta \vartheta(t) \quad (3.3)$$

The shape function,  $\psi(x)$ , may be any admissible function which adequately describes the behavior of the system and possesses derivatives of an order at least equal to those specified by the boundary conditions. The generalized

displacement,  $\vartheta(t)$ , is the solution to Duffing's equation. [Ref. 14: p. 34] The shape function which is chosen is the characteristic function for a clamped-free beam.

$$\psi(\xi) = \sqrt{2} \sin\left(\frac{\pi\xi}{2} - \frac{\pi}{4}\right) + \exp\left(-\frac{\pi}{2}\xi\right) + \exp\left(-\frac{\pi}{2}(1-\xi)\right) \quad (3.4)$$

where  $\xi$  is the beam coordinate, nondimensionalized with respect to the length,  $L$ , and varying between 0 and 1. [Ref 15: p. 439]

The boundary conditions for a cantilever beam are

$$\begin{aligned} \text{BC1: } & v(0,t) = 0 \\ \text{BC2: } & v'(0,t) = 0 \\ \text{BC3: } & v''(L,t) = 0 \\ \text{BC4: } & v'''(L,t) = 0 \end{aligned} \quad (3.5)$$

where (') indicates the derivative with respect to the spatial coordinate  $x$ .

The first boundary condition states that there is no displacement at the fixed end while the second states that its slope must also vanish here. The third and fourth boundary conditions state that there must be no moment and no shear forces at the free end. Applying the boundary conditions of Equation (3.5) to the shape function of Equation (3.4) gives only a 0.7% error in amplitude at the midpoint. [Ref 16: p. 1014]

The first and second derivatives of the shape function will be necessary in determining the coefficients for Duffing's equation. Subsequently,

$$\psi'(\xi) = \sqrt{2} \frac{\pi}{2} \cos\left(\frac{\pi\xi}{2} - \frac{\pi}{4}\right) - \frac{\pi}{2} \exp\left(-\frac{\pi}{2}\xi\right) + \frac{\pi}{2} \exp\left(-\frac{\pi}{2}(1-\xi)\right) \quad (3.6)$$

$$\psi''(\xi) = -\sqrt{2} \frac{\pi^2}{4} \sin\left(\frac{\pi\xi}{2} - \frac{\pi}{4}\right) + \frac{\pi^2}{4} \exp\left(-\frac{\pi}{2}\xi\right) + \frac{\pi^2}{4} \exp\left(-\frac{\pi}{2}(1-\xi)\right) \quad (3.7)$$

The principle of virtual displacements states that the combined virtual work of all forces must be zero. More explicitly this is stated as

$$\delta W_{nc} - \delta V + \delta W_{damp} + \delta W_{inert} = 0 \quad (3.8)$$

where  $\delta W_{nc}$  is the virtual work of nonconservative forces,  $\delta V$  is the change in strain energy of the system,  $\delta W_{damp}$  is the virtual work of damping forces, and  $\delta W_{inert}$  is the virtual work of inertia forces [Ref. 14: p. 34].

### 1. Mass Coefficient Determination

Solving for the virtual work of inertia forces will yield the mass term,  $m$ , of Duffing's Equation (3.1). Since the inertia force per unit length is distributed along the beam, the virtual work of inertia forces is

$$\begin{aligned} \delta W_{inert} &= \int_0^L -\rho A \ddot{v} \delta v \, dx \\ &= -\rho AL \int_0^1 \psi^2 \, d\xi \, \ddot{\vartheta} \delta \vartheta \end{aligned} \quad (3.9)$$

Using the values for density, area, and length of the beam contained in Table 3.1 and numerically integrating using MATHCAD (see Appendix B), the work done by inertia forces is

$$\delta W_{inert} = 1.0360 \times 10^{-1} \ddot{\vartheta} \delta \vartheta \quad (3.10)$$

Therefore, the mass coefficient,  $m$ , of Duffing's equation is 0.10360 slugs.

## 2. Stiffness Coefficients Determination

If a beam is modeled as shown in Figure 3.2 with coordinate axes  $x$ ,  $y$ , and  $z$  and corresponding displacements  $u$ ,  $v$ , and  $w$ , it can be shown [Ref. 17: p. 22] that the strain in the  $x$  direction is given by the following equation:

$$\epsilon_{xx} = \frac{\partial u}{\partial x} + \frac{1}{2} \left[ \left( \frac{\partial u}{\partial x} \right)^2 + \left( \frac{\partial v}{\partial x} \right)^2 + \left( \frac{\partial w}{\partial x} \right)^2 \right] \quad (3.11)$$

Assuming that all higher order terms are negligible except for  $(\partial v/\partial x)^2$  (small strain, large rotation assumption), the above equation becomes:

$$\epsilon_{xx} = \frac{\partial u}{\partial x} + \frac{1}{2} \left( \frac{\partial v}{\partial x} \right)^2 \quad (3.12)$$

Applying the classical Euler-Bernoulli assumption that cross sections are assumed to remain planar and normal to the centroidal axis after deformation [Ref. 18: p. 152], it can be seen from Figure 3.3 that

$$u = -y \tan \theta_z \quad (3.13)$$

$$\tan \theta_z = \frac{\Delta v}{\Delta x} \quad (3.14)$$

Subsequently

$$u = -y \frac{dv}{dx} \quad (3.15)$$

$$\frac{\partial u}{\partial x} = -y \frac{d^2 v}{dx^2} \quad (3.16)$$

Substituting Equation (3.16) into Equation (3.12) yields

$$\epsilon_{xx} = -y \frac{d^2v}{dx^2} + \frac{1}{2} \left( \frac{d^2v}{dx^2} \right)^2 \quad (3.17)$$

The expression for the strain energy of a beam undergoing transverse deflection is given by [Ref. 19: p. 169]

$$V = \frac{1}{2} \int_0^L \sigma_{xx} \epsilon_{xx} dx dA \quad (3.18)$$

Because the beam under study is not deflected so the material passes its yield point, it behaves as a Hookean material such that

$$\sigma_{xx} = E \epsilon_{xx} \quad (3.19)$$

Therefore the strain energy becomes

$$V = \frac{1}{2} E \int_0^L \epsilon_{xx}^2 dx dA \quad (3.20)$$

Squaring Equation (3.17) and substituting it into Equation (3.20) yields:

$$V = \frac{E}{2} \int_0^L \left[ y^2 \left( \frac{d^2v}{dx^2} \right)^2 - y \left( \frac{dv}{dx} \right)^2 \frac{d^2v}{dx^2} + \frac{1}{4} \left( \frac{dv}{dx} \right)^4 \right] dx dA \quad (3.21)$$

If the intersection of the y and z axes lies at the centroid then

$$\int y^2 dA = I_{zz} \quad (3.22)$$

$$\int y dA = 0 \quad (3.23)$$

Therefore, Equation (3.21) becomes:

$$V = \frac{EI}{2} \int_0^L \left( \frac{d^2v}{dx^2} \right)^2 dx + \frac{EA}{8} \int_0^L \left( \frac{dv}{dx} \right)^4 dx \quad (3.24)$$

Applying variational calculus, Equation (3.24) becomes

$$\delta V = EI \int_0^L \frac{d^2v}{dx^2} \frac{d^2\delta v}{dx^2} dx + \frac{EA}{2} \int_0^L \left( \frac{dv}{dx} \right)^3 \frac{d\delta v}{dx} dx \quad (3.25)$$

which can be written

$$\delta V = EI \int_0^L v'' (\delta v)'' dx + \frac{EA}{2} \int_0^L (v')^3 (\delta v)' dx \quad (3.26)$$

Substituting the derivatives of Equation (3.2) and (3.3) and substituting Equations (3.6) and (3.7) into Equation (3.26) yields

$$\delta V = EI \int_0^L (\psi'')^2 \vartheta \delta \vartheta dx + \frac{EA}{2} \int_0^L (\psi')^4 \vartheta^3 \delta \vartheta dx \quad (3.27)$$



Substituting in the values from Table 3.1 and numerically integrating using MATHCAD (See Appendix B), Equation (3.27) becomes

$$\delta V = 1.5433 \times 10^{-2} \delta \delta + 4.5943 \times 10^1 \delta^3 \delta \quad (3.28)$$

From Equation (3.28), the linear and nonlinear stiffness coefficients,  $k_1$  and  $k_3$ , are seen to be 0.015433 lbs/in and 45.943 lbs/in<sup>3</sup> respectively.

### 3. Damping Coefficient Determination

If the beam is assumed to be modelled by a linear single degree of freedom system the damping coefficient is given by

$$c_d = 2 \sqrt{k_1 m} \zeta \quad (3.29)$$

where:  $\zeta$  = viscous damping factor

The values for  $k_1$  and  $m$  were determined previously. In order to determine the viscous damping factor, the logarithmic decrement method was used [Ref. 14: p. 62]. The logarithmic decrement,  $\delta$ , is defined by

$$\delta = \ln \left( \frac{U_P}{U_Q} \right) = \frac{2 \pi \zeta N}{\sqrt{1 - \zeta^2}} \quad (3.30)$$

where:  $U_P$  = amplitude of motion at beginning of cycle

$U_Q$  = amplitude of motion after  $N$  cycles

$N$  = number of cycles

The above equation is used to solve for the viscous damping factor by displacing the tip of the beam and then measuring the two amplitudes,  $U_P$  and  $U_Q$ , and counting the number of cycles between the two measurements. These measurements were performed on an air table in the Flexible Spacecraft Simulator Laboratory of NPS as shown in Figures 3.4 and 3.5. The beam was horizontally mounted on the table and an air pad was attached to the tip of the beam. The tip was then deflected and the resulting motion achieved essentially without friction. The values for  $U_P$ ,  $U_Q$ , and  $N$  appear in Table 3.2. Using Equation (3.30), the average viscous damping factor,  $\zeta$ , was determined to be  $6.67 \times 10^{-3}$  or approximately 0.7%.

The virtual work of the damping forces is given by

$$\begin{aligned}\delta W_{\text{damp}} &= - \int_0^L c_d \dot{v} \delta v \\ &= -c_d \int_0^1 \psi^2 d\xi \dot{\vartheta} \delta \vartheta\end{aligned}\tag{3.31}$$

Substituting in the value for  $c_d$  obtained from Equation (3.29) and numerically integrating once again yields

$$\delta W_{\text{damp}} = 2.5654 \times 10^{-3} \dot{\vartheta} \delta \vartheta\tag{3.32}$$

Therefore, the damping coefficient,  $c$ , of Equation (3.1) is 0.0025654 slugs/s.

### C. THEORETICAL RESULTS

Appendix A contains the FORTRAN computer code used to numerically integrate the Duffing's equation which mathematically describes the motion of the flexible beam being studied. Table 3.3 summarizes the results of the previous section in which the coefficients of Equation (3.1) were determined. Equation (3.1) was then integrated using an amplitude of 3 lbs. (the force applied by the shaker) and a frequency of 5.6 Hz. The initial displacement and velocity chosen were 1 inch and 0 in/s, respectively. The results were then formatted to be read by the computer program "Chaos" developed by M. Sarigul Klijn [Ref. 1].

Qualitative tests for chaos are satisfied by the time series, Fourier spectrum, pseudo-phase plane and Poincare section. Figure 3.6 shows the time history of the acceleration of Equation (3.1). It shows no noticeable periodic behavior and this is confirmed in the Fourier spectrum of Figure 3.7. The power spectrum is made up of many frequencies with broad band characteristics. The pseudo-phase plane of Figure 3.8 was obtained using an embedding time of 10. This embedding time, consistent with the findings of Dvorak and Klaschka [Ref 9], yielded the least amount of bias. Notice that the trajectory frequently crosses itself and fills up a section of the phase space. The Poincare section, as shown in Figure 3.9, is also characteristic of damped chaotic systems with its cloud of unorganized points filling a section of the space. It was obtained by passing a plane through the three-dimensional pseudo-phase space at  $z = 0$ .

The quantitative tests for chaos were also performed. Figure 3.10 is a plot of the average Lyapunov exponent. This figure is obtained by time averaging the many computations of Equation (2.4) and then plotting them versus the

number of samples, 4096. The average Lyapunov exponent for this system is 0.949. This exponent is indicative of chaotic systems.

Figure 3.11 shows the plot from which the fractal correlation dimension is determined. As mentioned previously, the fractal correlation dimension is the asymptotic value obtained by plotting the slope of  $\log[C(r)]$  versus  $\log(r)$  for successively higher pseudo-phase space dimensions. It was determined to be approximately 2.4. Moon reports a value of 2.5 for his buckled beam experiment. [Ref. 2, p. 232]. The non-integer fractal correlation dimension is yet another indication of chaos in dynamic systems.

**TABLE 3.1      Beam Properties**

Density, $\rho$	0.101 lbm/in <sup>3</sup>	Modulus, E	10.4 x 10 <sup>6</sup> psi
Length, L	90.0 in	Area, A	0.24 in <sup>2</sup>
Thickness, t	0.080 in	Mom Inert, I	0.000128 in <sup>4</sup>
Width, w	3.0 in		

**TABLE 3.2      Logarithmic Decrement Values**

N	U <sub>p</sub> (in)	U <sub>Q</sub> (in)	$\zeta$
20	2.5625	1.0000	0.00749
20	2.3125	0.9375	0.00718
20	2.2500	0.9375	0.00697
20	2.6250	1.0625	0.00720
20	2.7500	1.1250	0.00711
25	2.2500	0.8125	0.00648
25	2.6250	0.8750	0.00699
25	2.5000	0.8750	0.00668
25	2.2500	0.8125	0.00648
25	2.2500	0.8125	0.00648
30	1.8125	0.6250	0.00565
30	2.6250	0.7500	0.00665
30	2.1875	0.6875	0.00614
30	1.9375	0.5625	0.00656
30	1.9375	0.6250	0.00600

**TABLE 3.3**      **Coefficients of Duffing's Equation**

$m = 1.0360 \times 10^{-1}$
$c = 2.5654 \times 10^{-3}$
$k_1 = 1.5433 \times 10^{-2}$
$k_3 = 4.5943 \times 10^1$

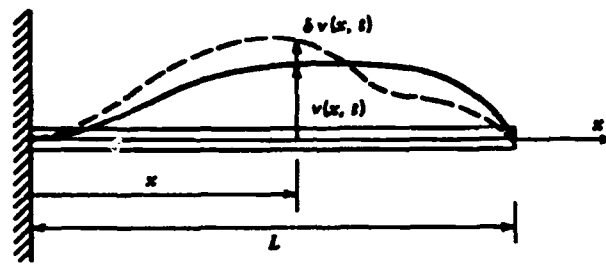


**Figure 3.1** Illustration of virtual displacements

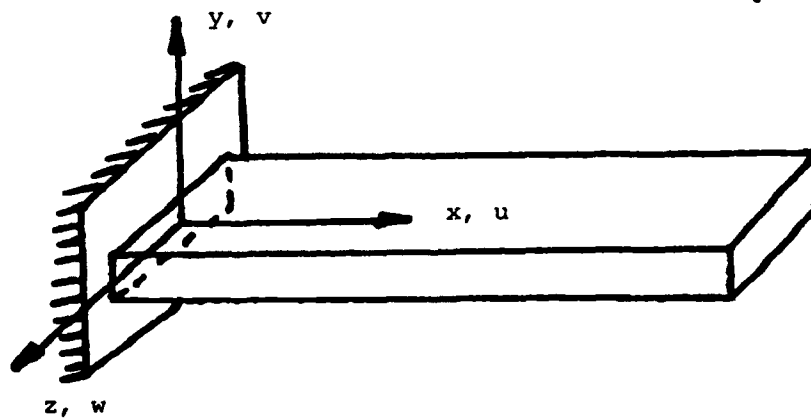


**Figure 3.2** Coordinates of a simple beam

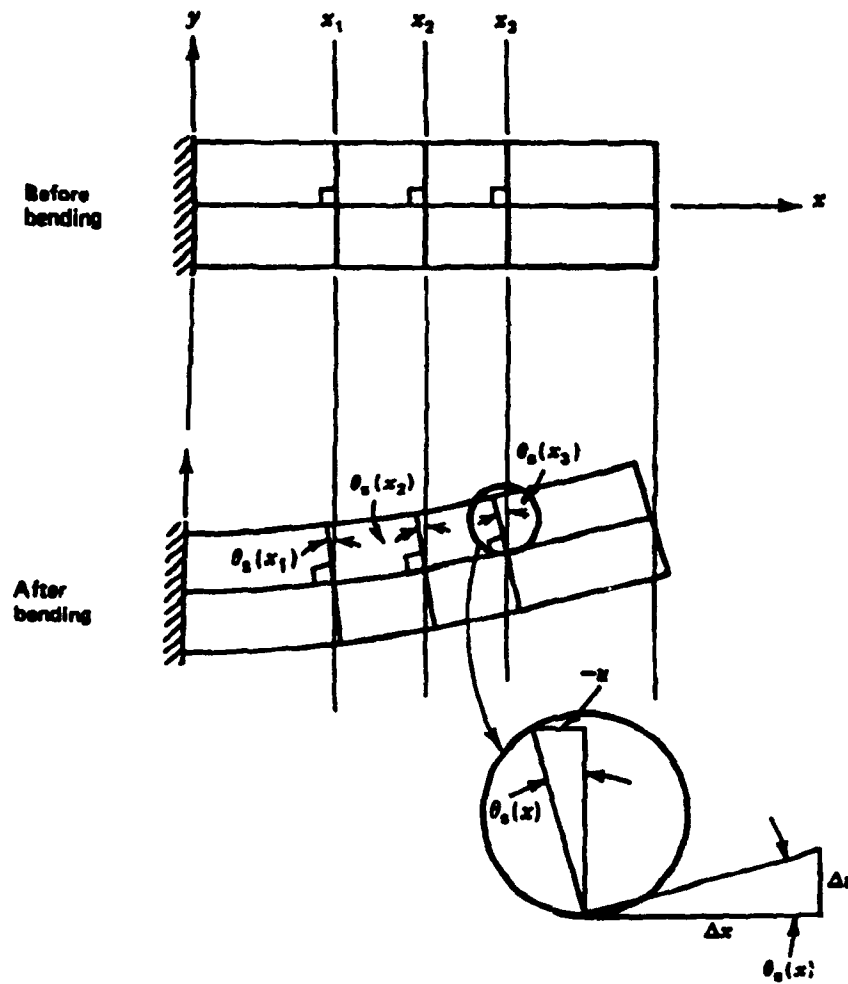


Figure 3.3 Kinematics of a simple beam

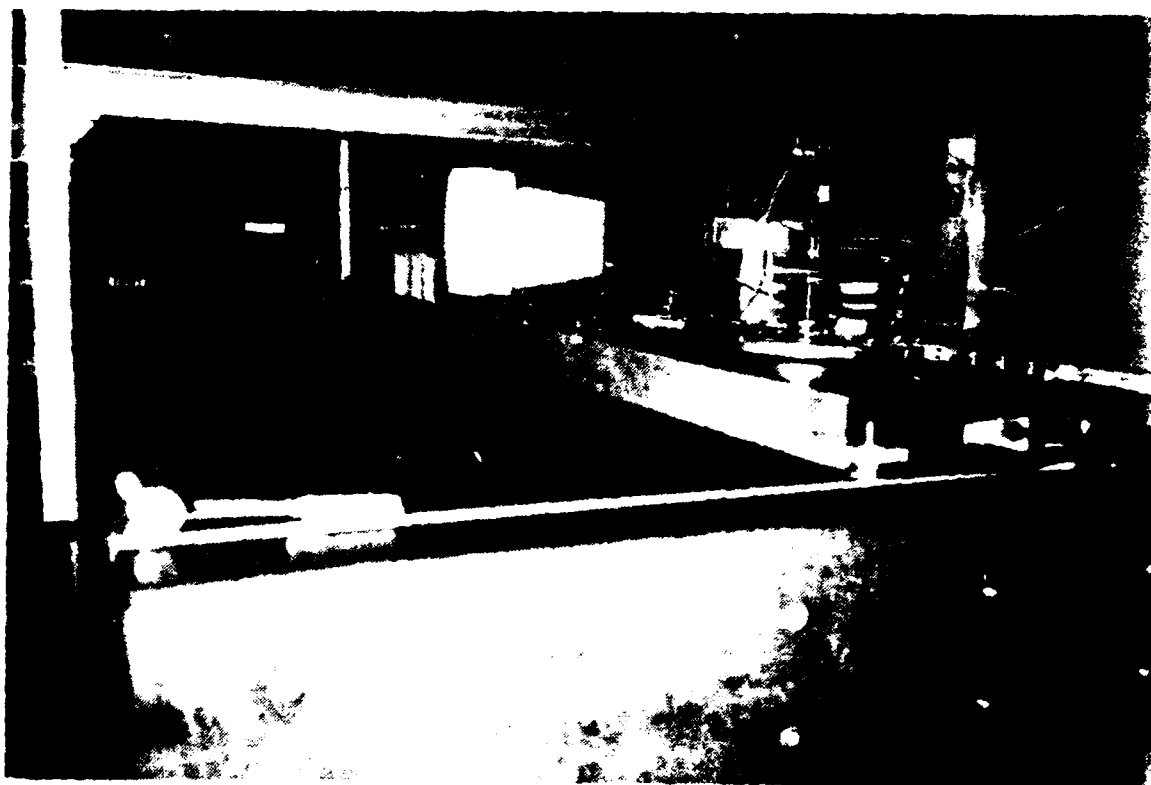
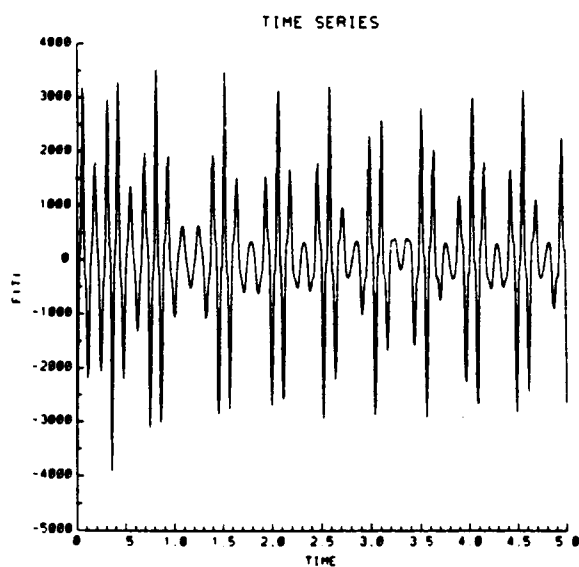


Figure 3.4 View 1 of beam on air table

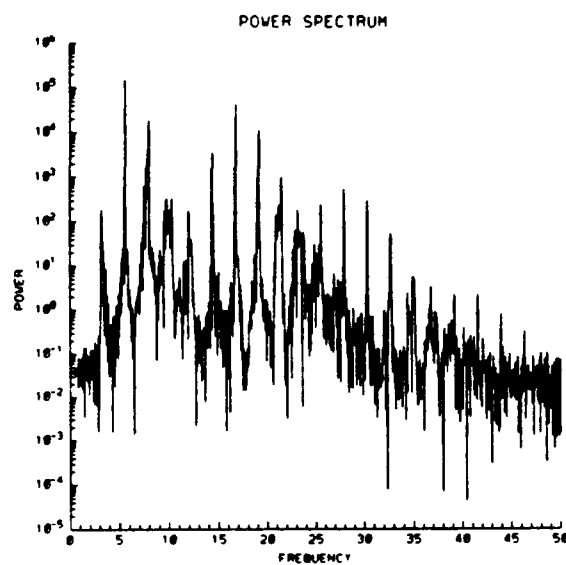




Figure 3.5 View 2 of beam on air table



**Figure 3.6 Time series of Duffing's Equation.**



**Figure 3.7 Fourier spectrum of Duffing's equation.**

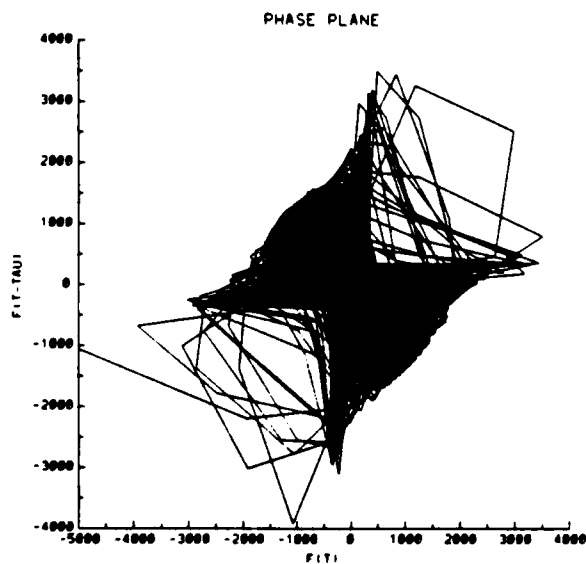


**Figure 3.8 Pseudo-phase plane of Duffing's Equation.**

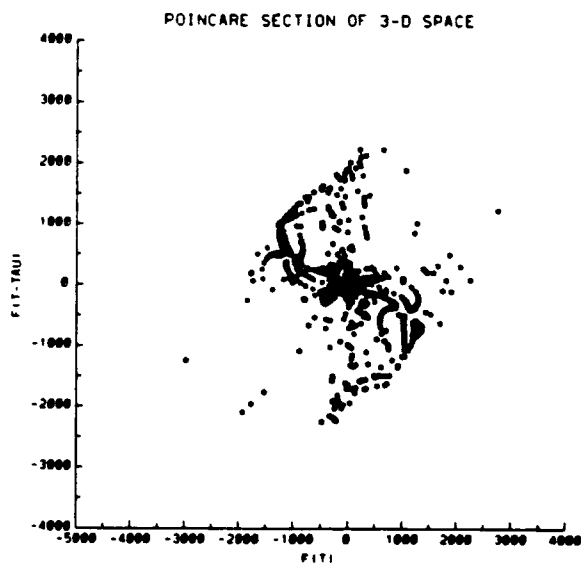


**Figure 3.9 Poincare section of Duffing's equation.**

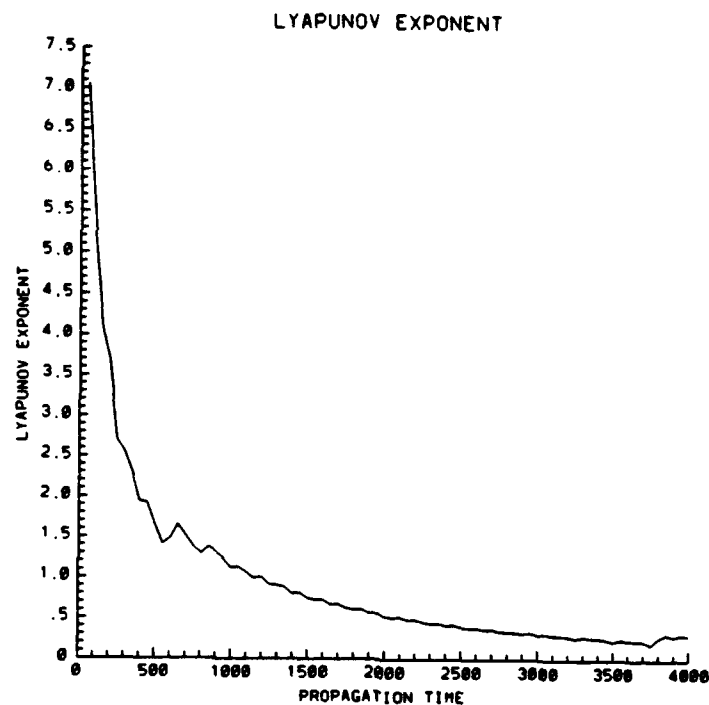


**Figure 3.10** Lyapunov Exponent of Duffing's equation.

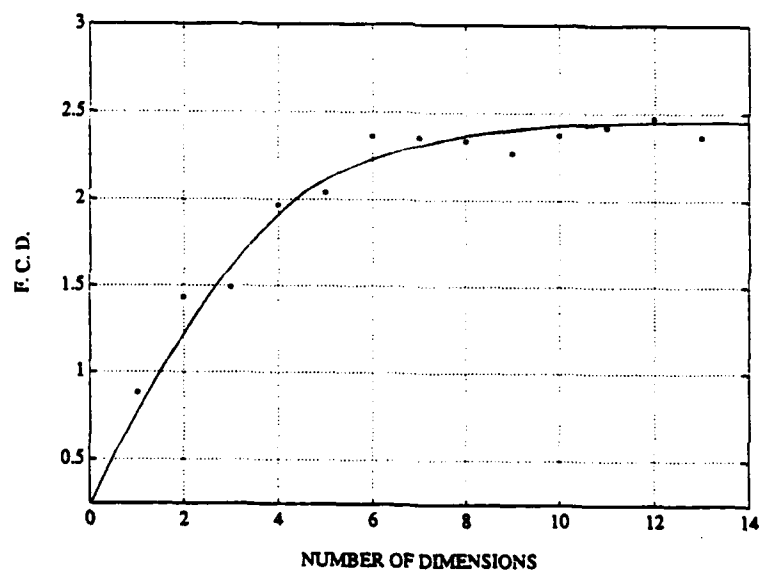


**Figure 3.11** Fractal Correlation Dimension of Duffing's equation

## **IV. EXPERIMENTAL ANALYSIS**

### **A. EXPERIMENTAL SET-UP**

The aluminum beam with properties listed in Table 3.1 is instrumented with strain gauges and an accelerometer as shown in Figure 4.1. The type of strain gauges used are one-quarter inch, 350 ohm, straight geometry gauges from the Micro Measurements Group. The accelerometer is a Sensotec model JTF flat pack. This accelerometer has a weight of one ounce, a peak range of  $\pm 5$  g's, a sensitivity of 10 mV/g, and a usable frequency range of DC to 150 Hz.

The beam is mounted vertically to an MB Dynamics Model PM500A Vibration Exciter. The outputs from the strain gauges and accelerometer are then fed into a bridge balancing box and amplifier. The bridge box is capable of handling four inputs, one from the accelerometer and three from the strain gauges. From the bridge box, the signal goes to an analog-to-digital converter. From there the acceleration and strain data is stored on a Zenith computer. Mechanical stops placed 58 inches up from the base prevent the beam from buckling past one and three-fourths inches on either side. (Figure 4.2)

### **B. EXPERIMENTAL PROCEDURE**

The accelerometer is placed at location A1 in Figure 4.1. The accelerometer and the three strain gauges are then connected to the data acquisition system. The beam is held in the upright vertical position in order to zero out all the readings from the gauges and the accelerometer using the bridge balancing circuit. The beam is then released while simultaneously starting the exciter. The exciter provides an excitation frequency of 5.6 Hz and

a displacement amplitude of one-quarter inch peak-to-peak. This procedure is then repeated twice, placing the accelerometer at locations A2 and A3. Strain gauge measurements at location S1, S2, and S3 are obtained for each run.

### **C. EXPERIMENTAL RESULTS**

The data from each of the runs is transferred into a format readable by the "Chaos" program. It is then analyzed using the techniques discussed in Chapter II. These results appear at the end of this chapter. As shown in Figures 4.3 through 4.10, the four qualitative tests for chaos seem to be met:

1. Erratic and unpredictable time histories from both accelerometers and strain gauges.
2. Multiple broadbanded power spectrum spikes.
3. Crossing trajectories and filled up pseudo-phase space.
4. A cloud of unorganized points in the Poincare section characteristic of lightly damped systems.

These results appear similar to the chaotic results obtained by Sarigul-Klijn [Ref. 1] in his analysis of helicopter flight test data using higher harmonic control.

The quantitative tests show that the location of the type of sensor chosen impacts whether or not chaotic motion is found. Strain gauges only indicate chaos if placed near the root, while accelerometers only indicate chaos if placed near the tip. Figures 4.11 through 4.14 are plots of the average Lyapunov exponents and fractal correlation dimensions. A summary of the Lyapunov exponents and fractal correlation dimensions for each sensor appear in Tables 4.1 and 4.2. The Lyapunov exponents are all positive for the strain gauges. For the accelerometers, the Lyapunov exponent diminishes as the accelerometer is placed closer to the root. This indicates that measuring

accelerations near the root reduces the chances of obtaining chaotic results. This is anticipated since the beam does not experience large deflections in this area and can be characterized by linear equations. Likewise, the fractal correlation dimensions of the sensors indicate that accelerometers should be placed closer to the tip and strain gauges closer to the root. The accelerometer nearest the root has an integer fractal correlation dimension, like that of a non-chaotic system. The two nearer to the tip have non-integer fractal dimensions, characteristic of chaotic systems. Conversely, the two strain gauges near the root have non-integer fractal dimensions, while the one closer to the tip has an integer fractal dimension.

**TABLE 4.1      Lyapunov exponents**

S1	0.272	A1	0.364
S2	0.237	A2	0.0397
S3	0.390	A3	-0.0282

**TABLE 4.2      Fractal Correlation Dimensions**

S1	4.3	A1	4.4
S2	4.4	A2	4.4
S3	4.0	A3	4.0

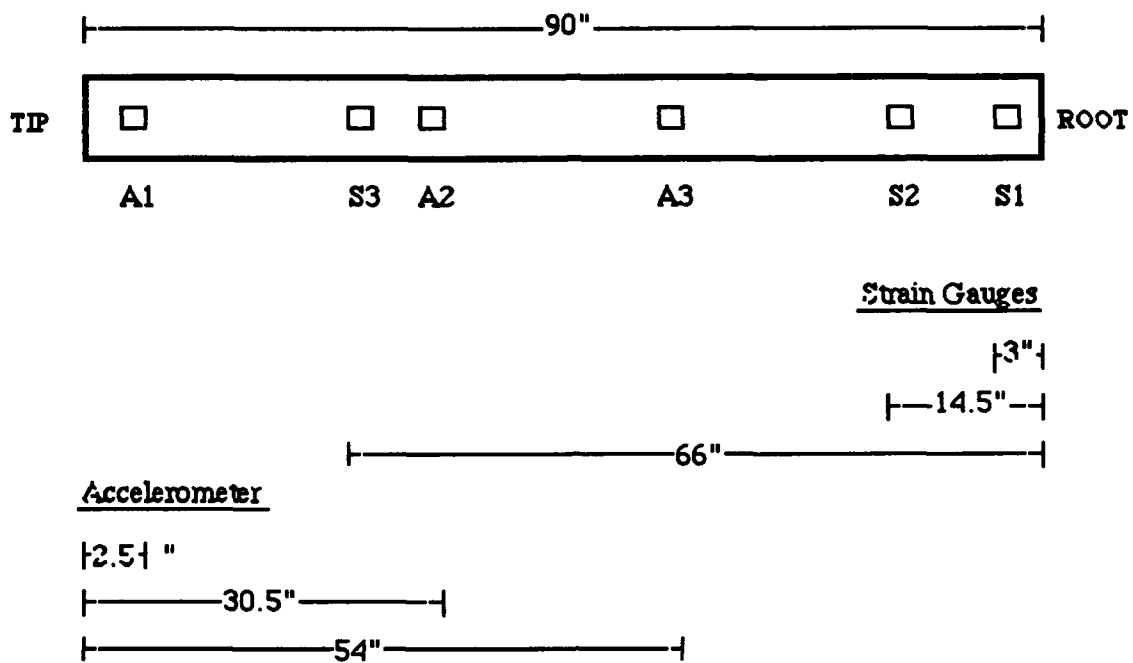


Figure 4.1 Sensor Locations

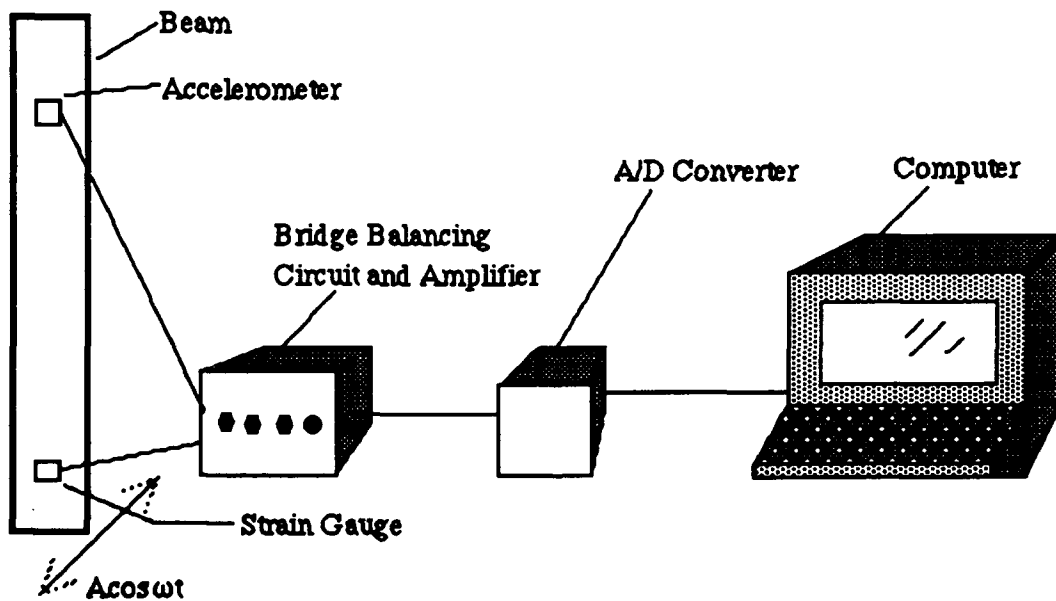
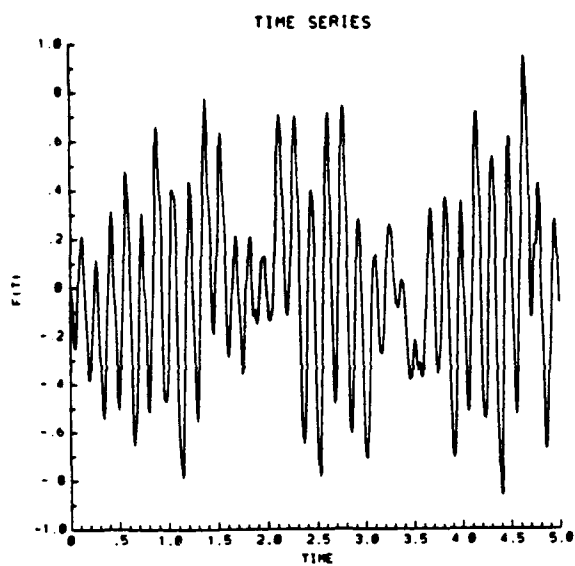
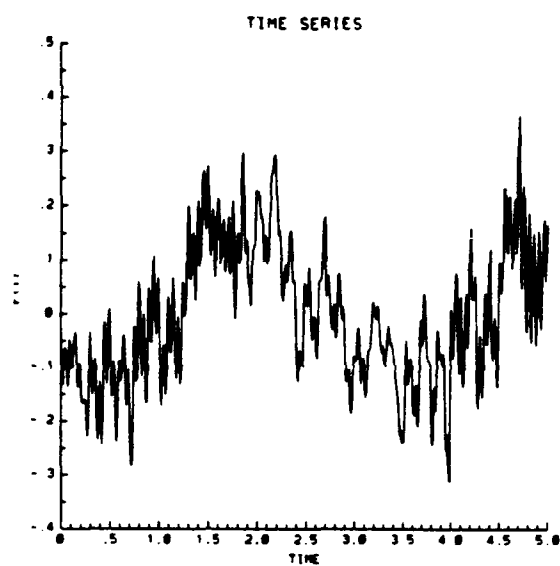


Figure 4.2 Experimental Set-up

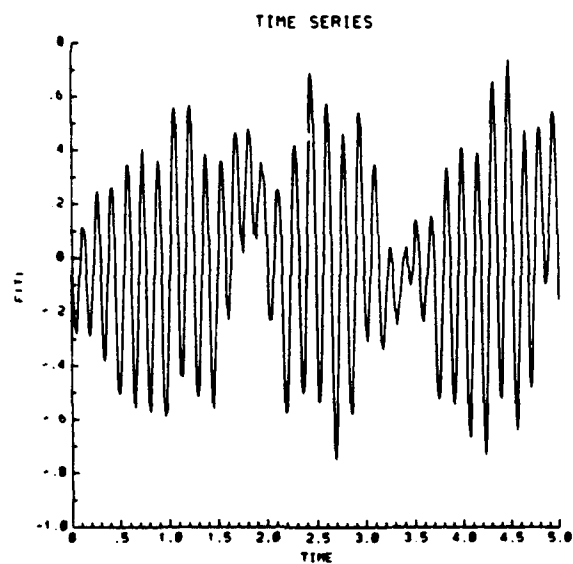




(a)



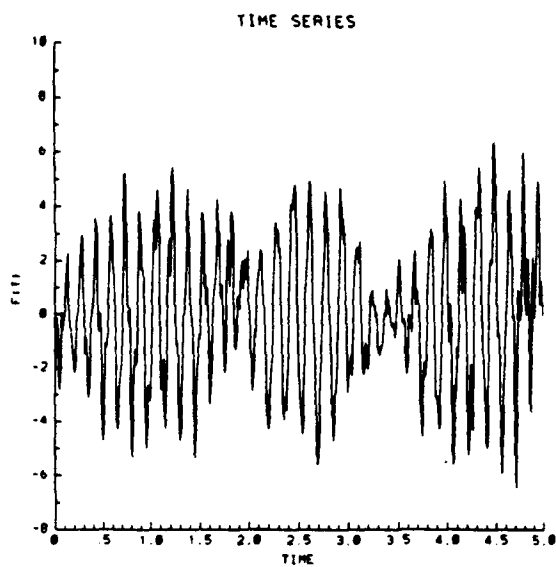
(b)



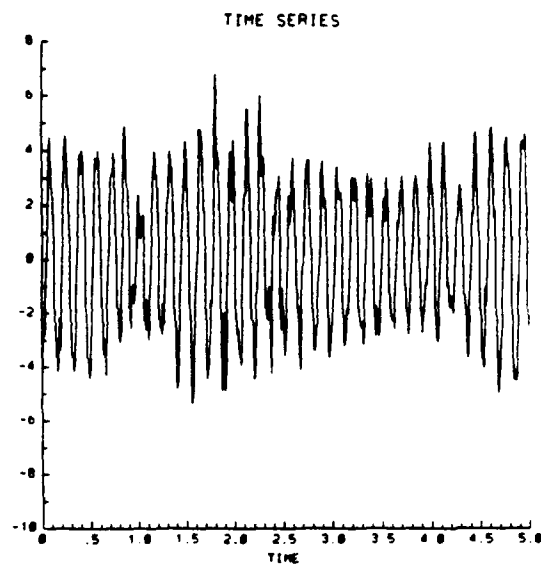
(c)

**Figure 4.3 Time series of strain gauges**

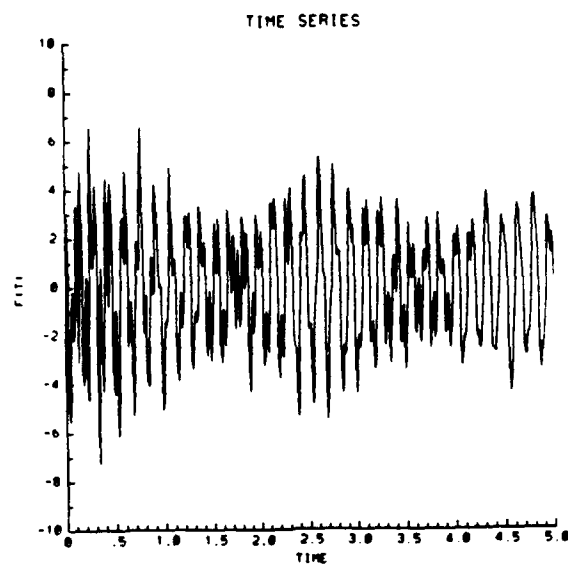
(a) S1 (b) S2 (c) S3



(a)



(b)



(c)

**Figure 4.4 Time series of accelerometers**

(a) A1 (b) A2 (c) A3

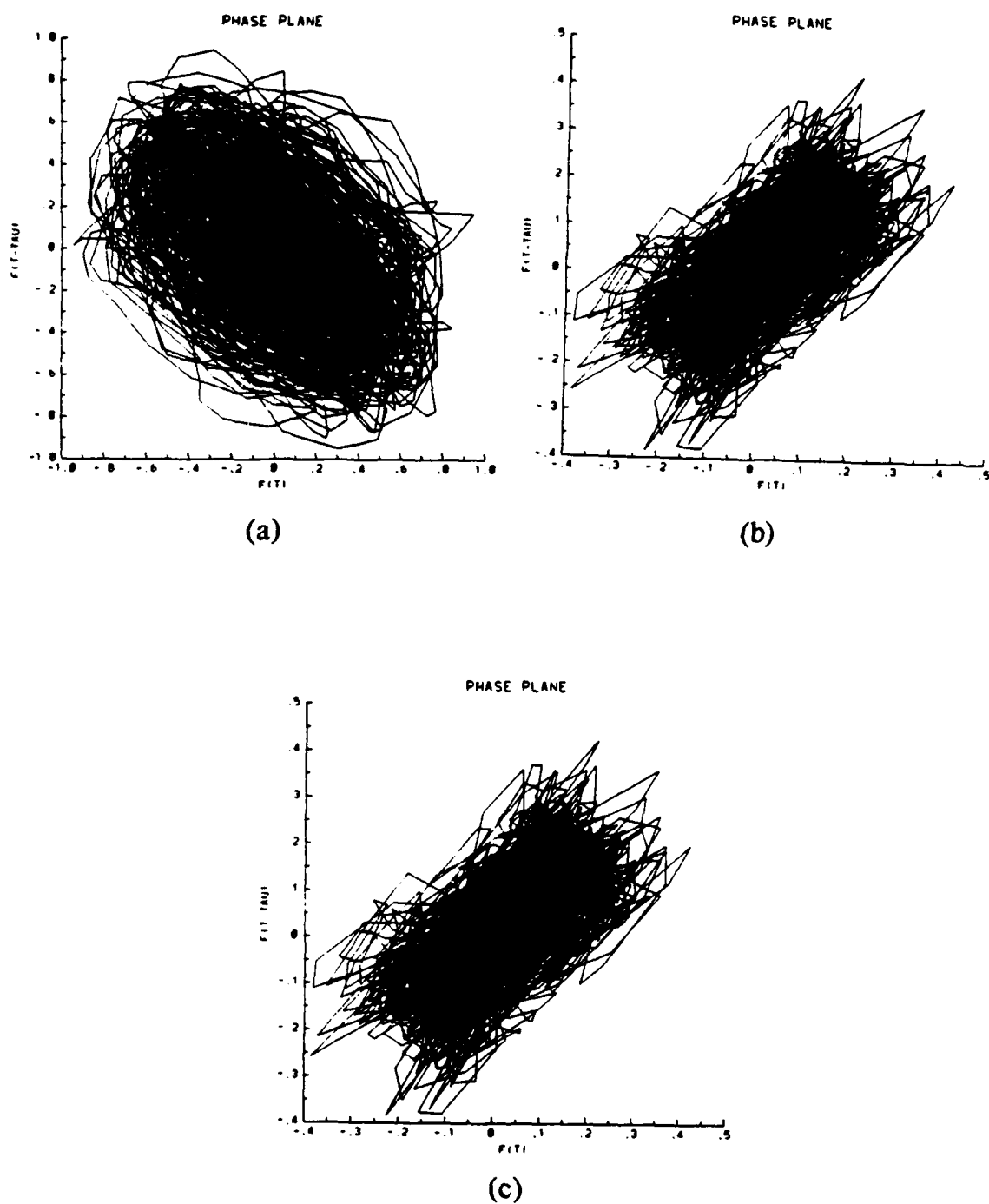
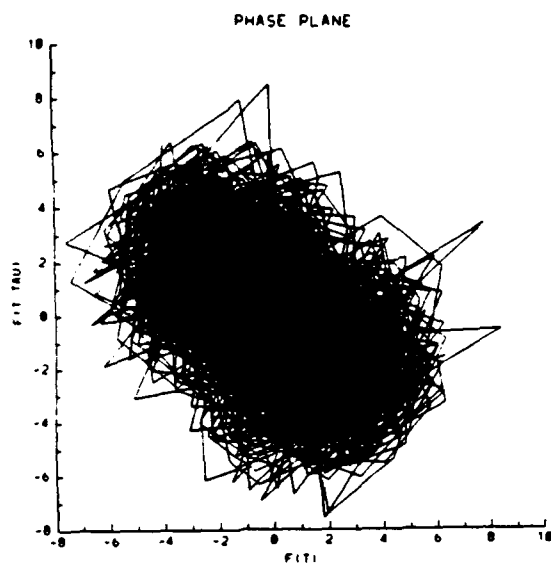
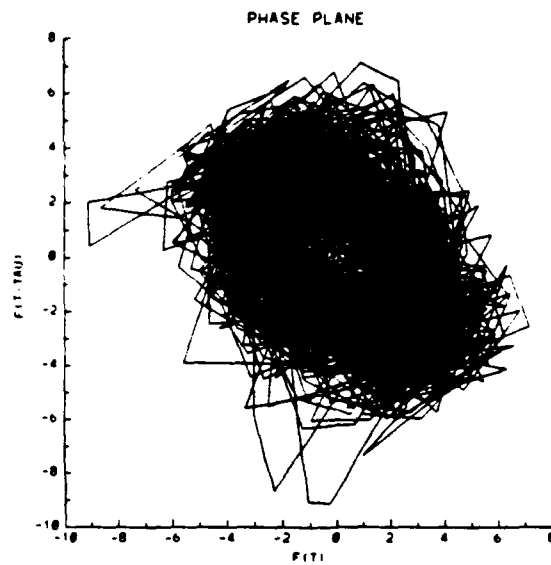


**Figure 4.5 Pseudo-phase planes of strain gauges**

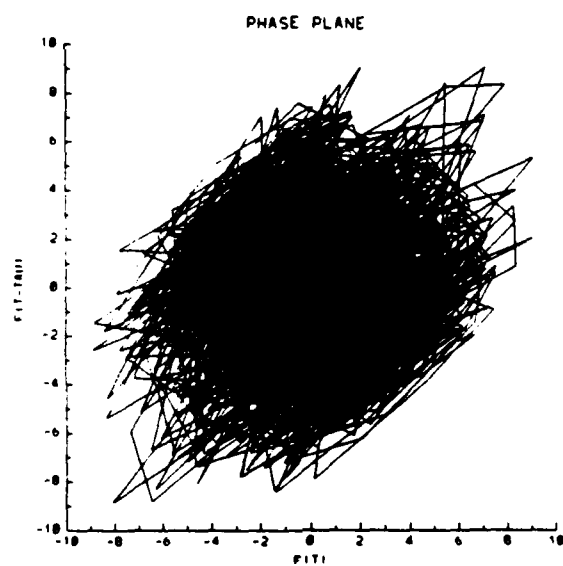
(a) S1 (b) S2 (c) S3



(a)



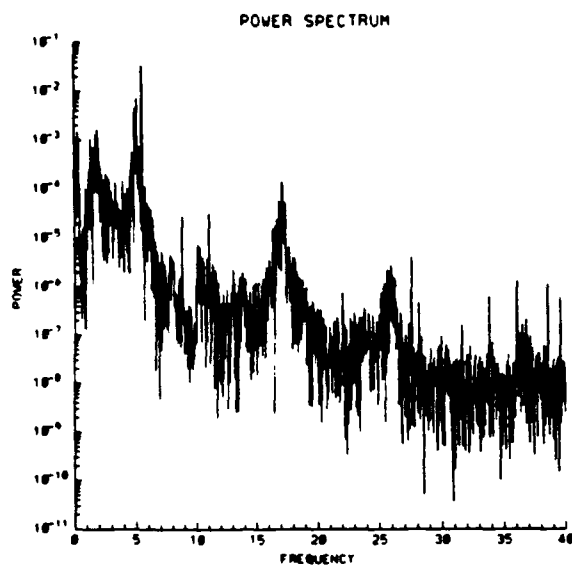
(b)



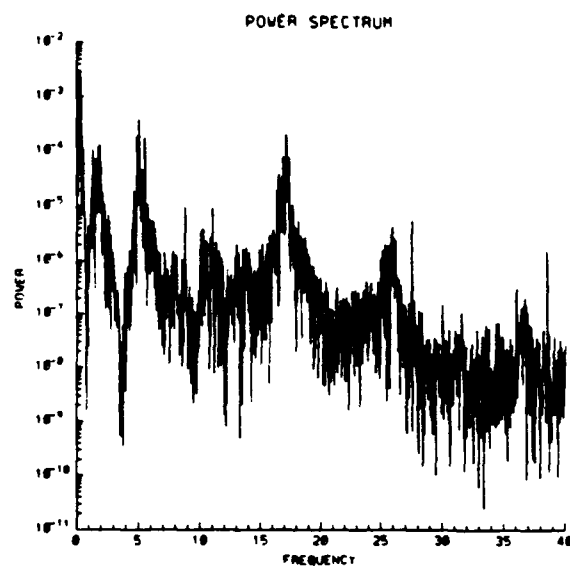
(c)

**Figure 4.6 Pseudo-phase planes of accelerometers**

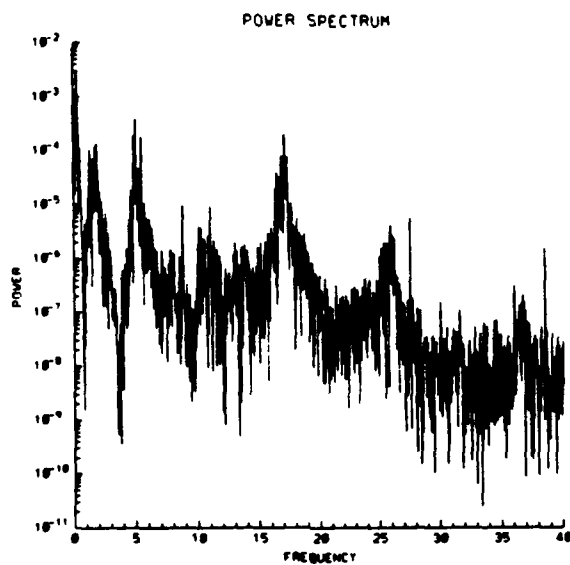
(a) A1 (b) A2 (c) A3



(a)



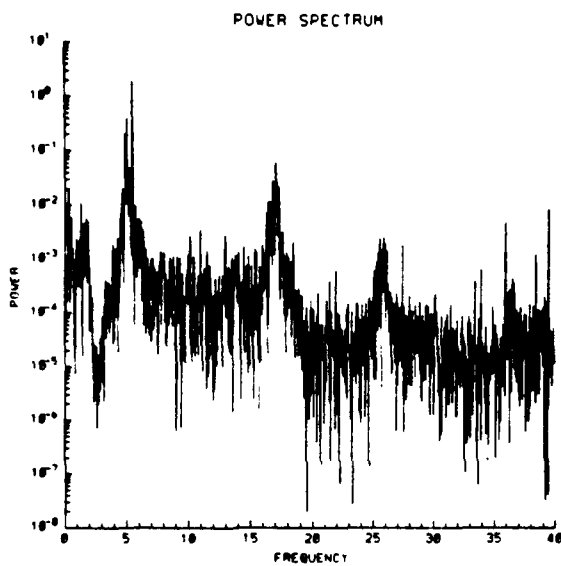
(b)



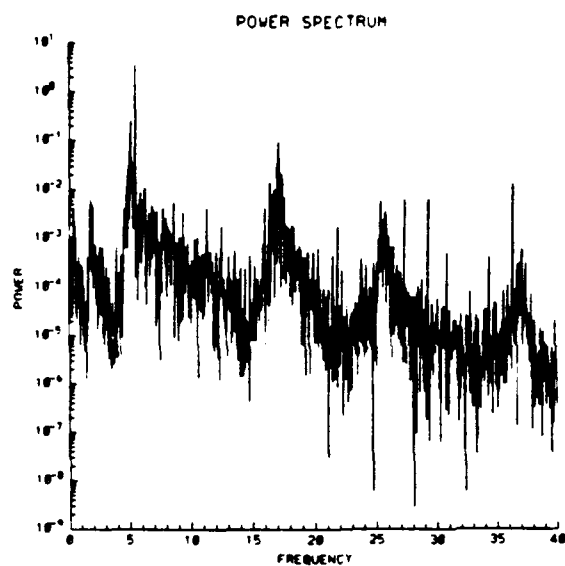
(c)

**Figure 4.7 Fourier spectrums of strain gauges**

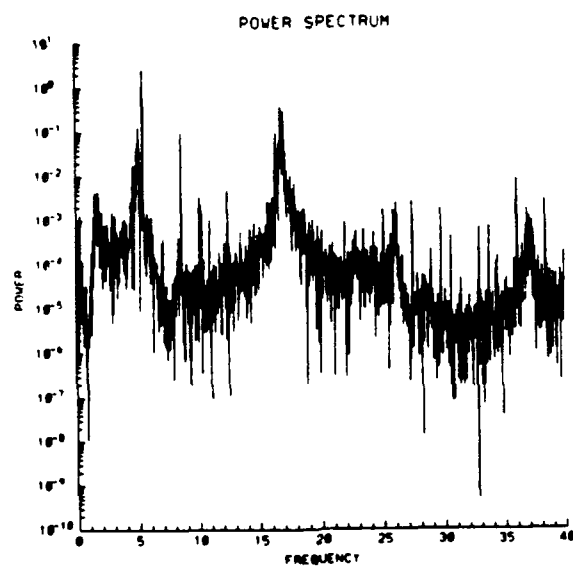
(a) S1 (b) S2 (c) S3



(a)



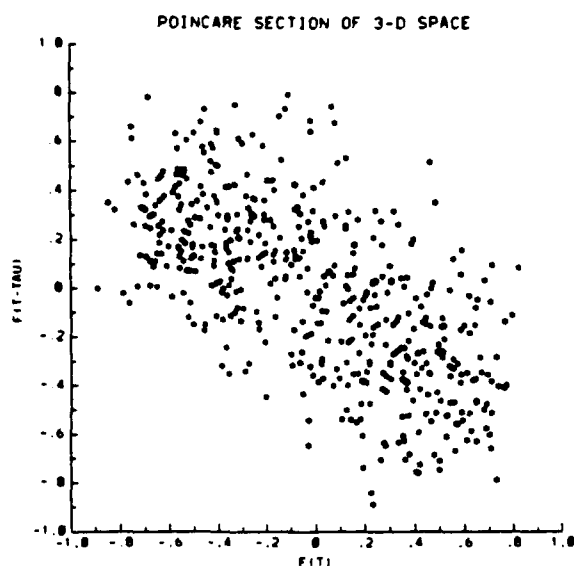
(b)



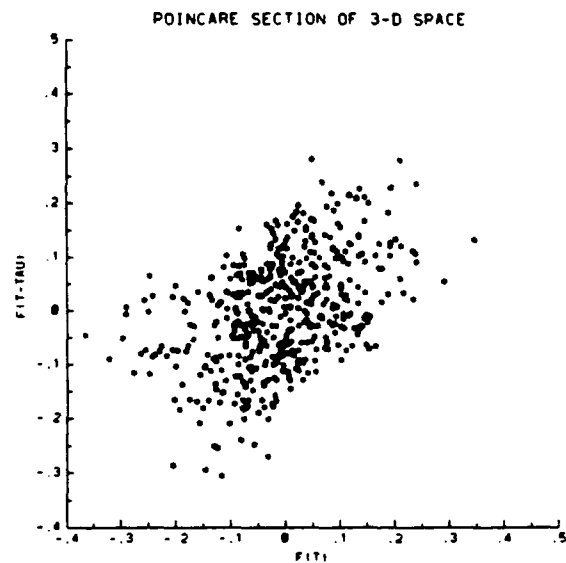
(c)

**Figure 4.8 Fourier spectrums of accelerometers**

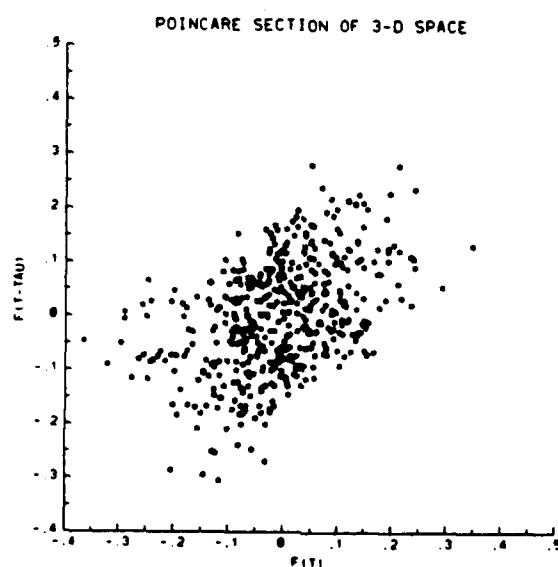
(a) A1 (b) A2 (c) A3



(a)



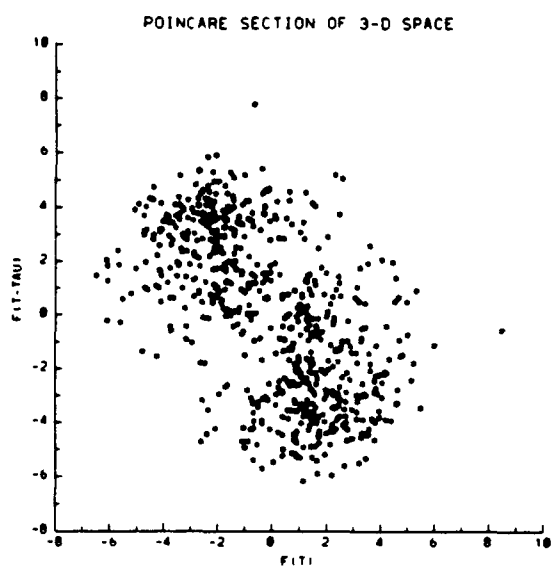
(b)



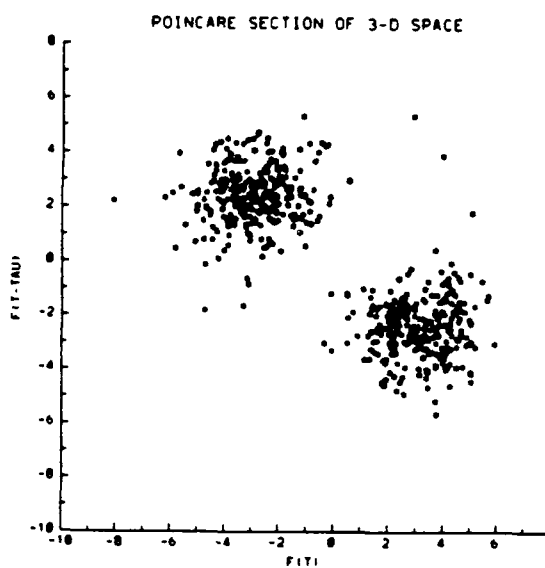
(c)

**Figure 4.9 Poincare sections of strain gauges**

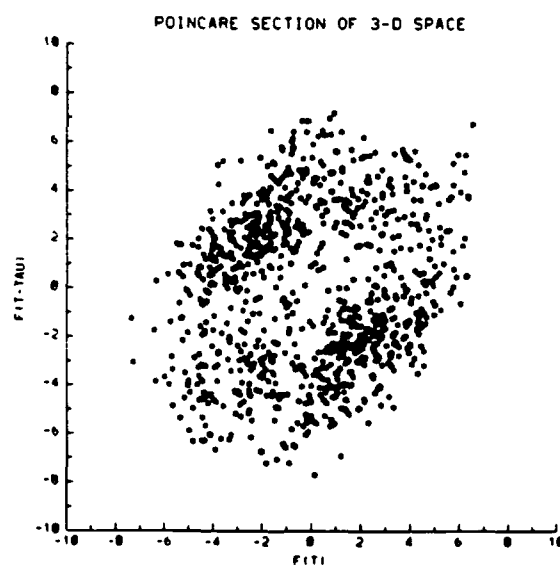
(a) S1 (b) S2 (c) S3



(a)



(b)



(c)

**Figure 4.10 Poincare sections of accelerometers**

(a) A1 (b) A2 (c) A3



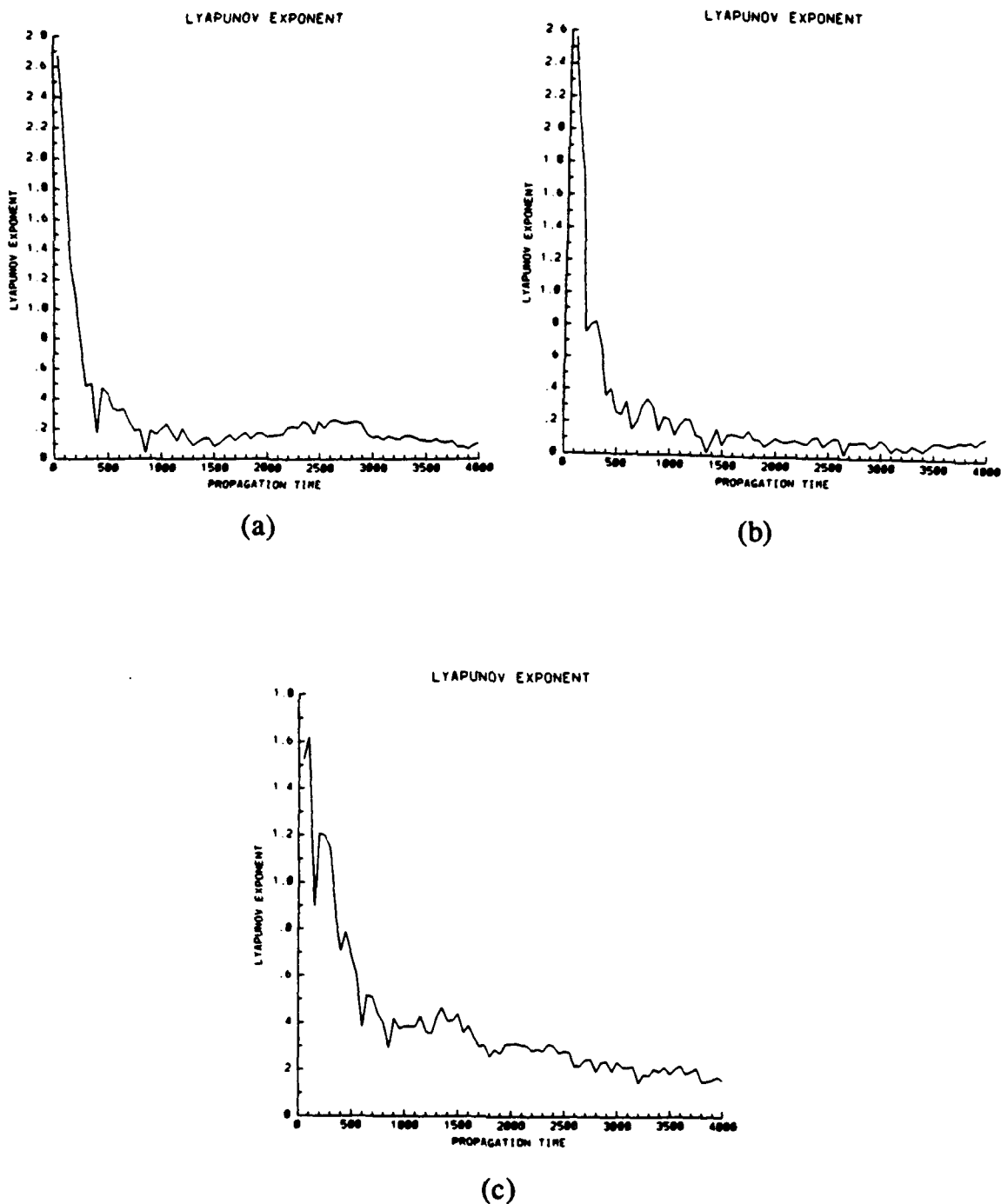
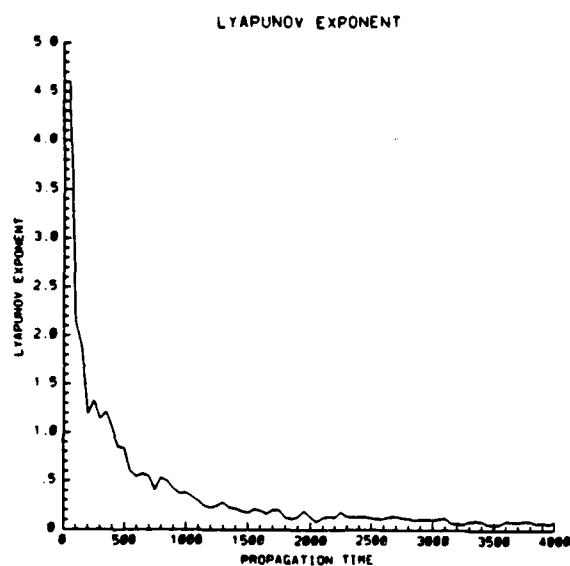
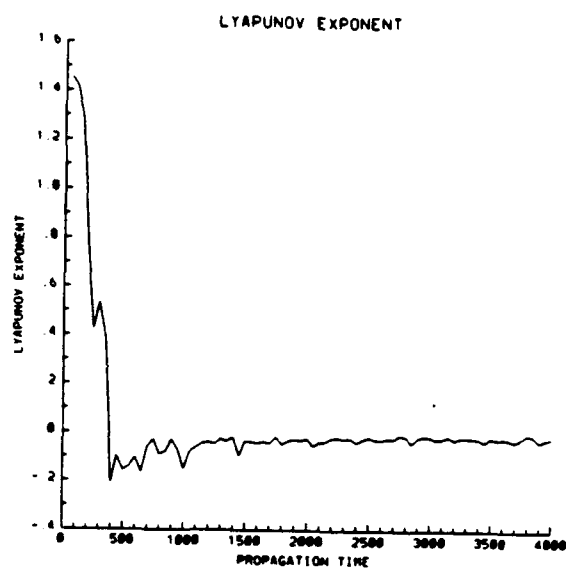


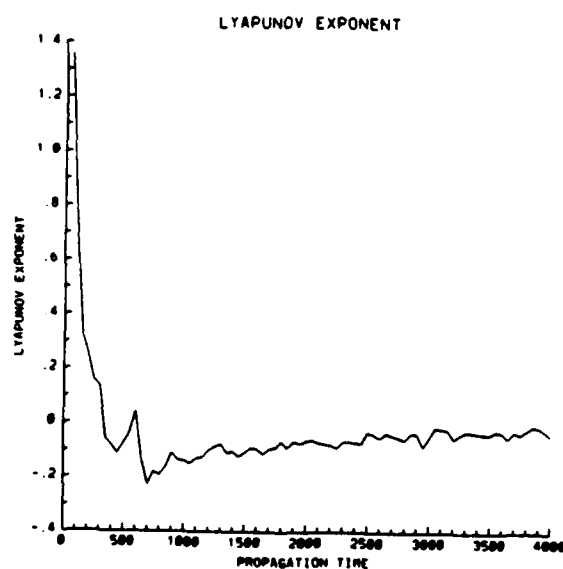
**Figure 4.11**      **Average Lyapunov exponents of strain gauges**  
 (a) S1   (b) S2   (c) S3



(a)

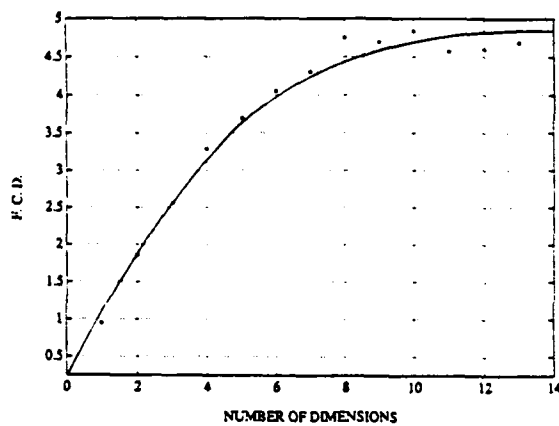


(b)

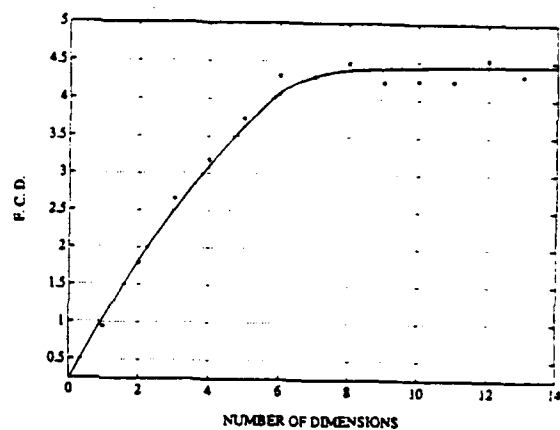


(c)

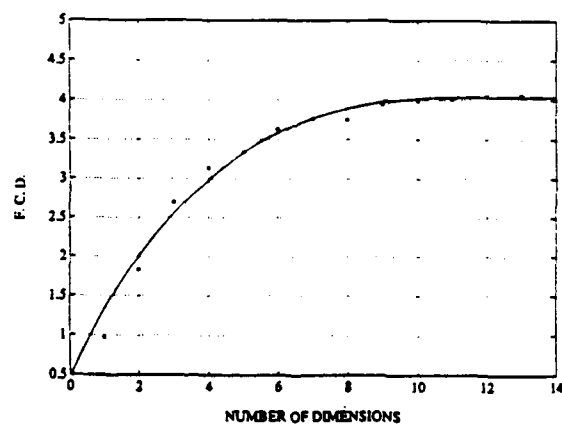
**Figure 4.12**      **Average Lyapunov exponents of accelerometers**  
 (a) A1    (b) A2    (c) A3



(a)



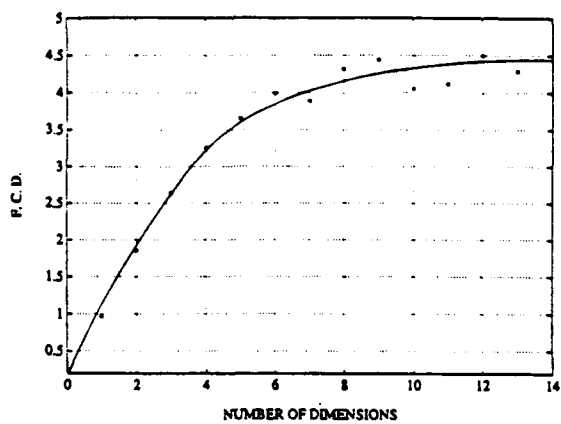
(b)



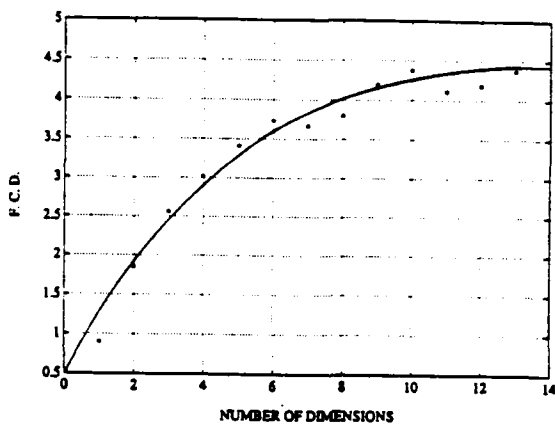
(c)

**Figure 4.13 Fractal correlation dimension of strain gauges**

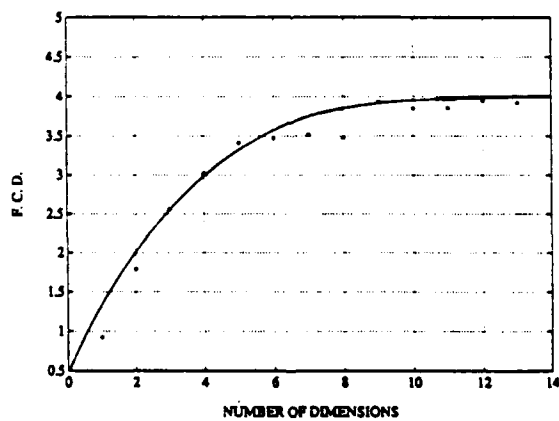
(a) S1 (b) S2 (c) S3



(a)



(b)



(c)

**Figure 4.14 Fractal correlation dimension of accelerometers**  
 (a) A1 (b) A2 (c) A3

## V. CONCLUSIONS AND SCOPE FOR FUTURE RESEARCH

For the first time geometric and topological methods of chaos were applied to data obtained simultaneously by accelerometers and strain gauges. It was determined that data from both accelerometers and strain gauges provided similar indications to the presence of chaos when analyzed using time series, Fourier spectrums, pseudo-phase planes, and Poincare sections. Using these techniques, both types of sensors indicated chaos without regard to the location of the sensor. However, the Lyapunov exponents and fractal correlation dimensions indicated that chaotic motion is only detected by accelerometers if they are placed near the tip and that chaotic motion is only detected by strain gauges if they are placed near the root.

The presence of chaos in highly flexible spacecraft structures was also investigated. It was determined that the geometric nonlinearities of these structures may result in chaotic vibrations and dynamic instabilities. These instabilities may then affect control mechanisms of the spacecraft. Further analysis could be performed in using the geometric and topological methods of chaos to analyze the effectiveness of these mechanisms to adequately control the spacecraft and provide improvements into the way the control is performed. Chaotic methods may also have an application in updating the linear finite elements models of flexible space structures with more accurate nonlinear models.

## APPENDIX A

```

*****
*
*  TITLE:      DUFFING
*  DATE:       07 DEC 1991
*  AUTHOR:     ROBERT G. VAUGHAN
*  SYSTEM:     VAX
*  COMPILER:   MASP
*  DESCRIPTION:
*  This program solves Duffing's equation
*
*       $m \frac{d^2x}{dt^2} + c \frac{dx}{dt} + k_1 x + k_3 x^3 = A \cos(\omega t)$ 
*
*  by transforming it into two ordinary differential equations
*
*       $\frac{dx}{dt} = y$ 
*
*       $\frac{dy}{dt} = A \cos(\omega t) - c y - k_1 x - k_3 x^3$ 
*
*  and using a fourth order Runge-Kutta Scheme to integrate to
*  find the displacement, x, and the velocity, y.
*
*  The amplitude and frequency of the forcing function, the step
*  size for integration, the number of integration steps, and the
*  initial values for displacement and velocity are entered in
*  that order in a data file titled "DUFFINIT." The data file
*  titled "DUFFOUT" contains the integrated values for displacement
*  and velocity in a format compatible with the program "CHAOS"
*  by M. Sarigul-Elijn.
*
*  To alter this program to solve an equation other than Duffing's
*  above, the parameter, NE, must be changed to correspond to the
*  number of ODE's and the subroutine "DIFFEQ" must be changed
*  to include the proper equations.
*
*  Two subroutines are employed.
*      DIFFEQ calculates the values for the ODE's
*      RK4 is the Runge-Kutta routine
*
*  As written the program does not use an adaptive step-size
*
*  The variables are defined as follows:
*      NE - the number of ODE's in the system
*      NS - the number of steps (iterations) to be performed
*      H - the desired stepsize
*      A - amplitude of the forcing function
*      F - frequency of the forcing function
*      TIME, T - time
*      I, INDEX - integer counters
*      X - an array corresponding to the independent variables,
*          i.e. X(1)=X, X(2)=Y, etc.
*      XDOT - an array corresponding to the ODE's
*
*****

PROGRAM DUFFING

PARAMETER (NE=2)
IMPLICIT DOUBLE PRECISION(A-H,X,N,O-Z)
CHARACTER*7 DUMMY
DIMENSION X(NE),XDOT(NE)

```

```

OPEN(7,FILE='DUFFINIT',STATUS='OLD')
OPEN(8,FILE='DUFFOUT',STATUS='OLD')

TIME=0.0D0
DUMMY=' A1234A'

READ(7,*) A,F,H,NS
DO 5 I=1,NE
    READ(7,*) X(I)
5    CONTINUE

WRITE(8,6) A,F
WRITE(8,7) H,NS
WRITE(8,8) X(1),X(2)

6    FORMAT (1X,'FORCING FUNCT AMPLITUDE = ',F4.1,5X,'FREQ = ',F6.3)
7    FORMAT (1X,'STEP SIZE = ',F6.4,5X,'NUMBER OF STEPS = ',I5)
8    FORMAT (1X,'INIT DISP = ',F4.1,5X,'INIT VEL = ',F4.1)

CALL DIFFEQ(X,XDOT,A,F,TIME)
WRITE(8,100) DUMMY,TIME,X(1),X(2),XDOT(2)

DO 15 I=1,NS
    DO 10 INDEX=1,4
        CALL DIFFEQ(X,XDOT,A,F,TIME)
        CALL RK4(TIME,X,XDOT,H,INDEX)
10    CONTINUE
    WRITE(8,100) DUMMY,TIME,X(1),X(2),XDOT(2)
15    CONTINUE
100   FORMAT(A7, F6.3, E11.4, 2E12.4)

STOP
END

*****
SUBROUTINE RK4(T,X,XDOT,H,INDEX)
*   This subroutine performs numerical integration using 4th order
*   Runge-Kutta methods.  It was developed by I.M. Ross.

PARAMETER(NE=2)
IMPLICIT DOUBLE PRECISION(A-H,K,M,O-Z)
DIMENSION X(NE),XDOT(NE),SAVED(NE),SAVEX(NE)

GO TO (1,2,3,4),INDEX
1    DO 10 I=1,NE
        SAVEX(I)=X(I)
        SAVED(I)=XDOT(I)
10   X(I)=SAVEX(I)+0.5D0*H*XDOT(I)
    T=T+0.5D0*H
    RETURN

```

```

2      DO 20 I=1,NE
          SAVED(I)=SAVED(I)+2.0D0*XDOT(I)
20     X(I)=SAVEX(I)+0.5D0*H*XDOT(I)
          RETURN

3      DO 30 I=1,NE
          SAVED(I)=SAVED(I)+2.0D0*XDOT(I)
20     X(I)=SAVEX(I)+H*XDOT(I)
          T=T+0.5D0*H
          RETURN

4      DO 40 I=1,NE
40     X(I)=SAVEX(I)+H/6.0D0*(SAVED(I)+XDOT(I))
          RETURN

```

END

\*\*\*\*\*

SUBROUTINE DIFFEQ(X,XDOT,A,F,T)

\* This subroutine obtains values for the ODE's for Duffing's  
 \* equation and must be changed for a new system of equations.

```

PARAMETER(NE=2)
IMPLICIT DOUBLE PRECISION(A-H,K,M,O-Z)
DIMENSION X(NE),XDOT(NE)

```

PI=4.0D0\*DATAN(1.0D0)

\* Be Careful of units!      K1 = Lbf/in.      K3 = Lbf/in^3  
 \*                              M = slugs              C = slugs/s

```

M=1.0360D-01
C=2.5654D-03
K1=1.5433D-02
K3=4.5943D+01

```

\* Divide M by 12 in/ft so that XDOT(2) has units in/s^2  
 M=M/12.0D0

```

XDOT(1)=X(2)
XDOT(2)=(A*COS(F*2.0D0*PI*T)-C/12.0D0*X(2)-K1*X(1)-K3*X(1)**3)/M

```

RETURN  
 END



# APPENDIX B

$$m := \int_0^1 \left[ \sqrt{2} \cdot \sin \left[ \pi \cdot \frac{x}{2} - \frac{\pi}{4} \right] + \frac{-\pi \cdot x}{2} + \frac{-\pi}{2} \cdot (1-x) \right]^2 dx$$

$$m = 1.388248302957508$$

$$k3 := \int_0^1 \left[ \sqrt{\frac{\pi}{2}} \cdot \cos \left[ \pi \cdot \frac{x}{2} - \frac{\pi}{4} \right] - \frac{\pi}{2} \cdot \frac{-\pi \cdot x}{2} + \frac{\pi}{2} \cdot \frac{-\pi}{2} \cdot (1-x) \right]^4 dx$$

$$k3 = 26.837183422538524$$

$$k1 := \int_0^1 \left[ \frac{\sqrt{2}}{4} \cdot \pi \cdot \sin \left[ \pi \cdot \frac{x}{2} - \frac{\pi}{4} \right] + \frac{\pi}{4} \cdot \left[ \frac{-\pi \cdot x}{2} \right] + \frac{\pi}{4} \cdot \left[ \frac{-\pi}{2} \cdot (1-x) \right] \right]^2 dx$$

$$k1 = 8.451750332536703$$

## LIST OF REFERENCES

1. Sarigul-Klijn, M., "Application of Chaos Methods to Helicopter Vibration Reduction Using Higher Harmonic Control," Ph.D. Dissertation, Naval Postgraduate School, Monterey, California, March 1990.
2. Moon, F., *Chaotic Vibrations*, John Wiley and Sons, New York, 1987.
3. Crutchfield, J., Farmer, J., Packard, N., and Shaw, R., "Chaos," *Scientific American*, V. 255, December 1986, pp. 46-57.
4. Gleick, J., *Chaos: Making a New Science*, Viking Penguin, New York, New York, 1987.
5. Moon, F., and Li, G., "Experimental Study of Chaotic Vibrations in a Pin Jointed Space Truss Structure," *AIAA Journal*, V. 28, No. 5, May 1990, pp. 915-921.
6. Walters, W., "Dynamic Analysis of the Low Power Atmospheric Compensation Experiment (LACE) Spacecraft," Masters Thesis, Naval Postgraduate School, Monterey, California, June, 1990.
7. Moon, F., and Shaw, S., "Chaotic Vibrations of a Beam with Nonlinear Boundary Conditions," *International Journal of Nonlinear Mechanics*, Vol. 18, No. 6, 1983, pp. 465-477.
8. Thompson, J., and Stewart, H., *Nonlinear Dynamics and Chaos*, John Wiley and Sons, New York, 1986.
9. Dvorak, I., and Klaschka, J., "Modification of the Grossberger-Procaccia Algorithm for Estimating the Correlation Exponent of Chaotic Systems with High Embedding Dimension," *Physic Letters A*, Vol. 145, No. 5, 16 April 90, pp. 225-231.
10. De Souza-Machado, S., Rollins, R., Jacobs, D., and Hartman, J., "Studying Chaotic Systems Using Microcomputer Simulations and Lyapunov Exponents," *American Journal of Physics*, V. 58, April, 1990, pp. 321-329.
11. Wolf, A., Swift, J., Swinney, H., and Vastano, J., "Determining Lyapunov Exponents From A Time Series," *Physica D*, vol. 16, 1985, pp. 285-317.

12. Tobochnik, J., and Gould, H., "Quantifying Chaos," *Computers in Physics*, Nov-Dec, 1989, pp. 86-90.
13. Moon, F., and Li, G., "The Fractal Dimension of the Two Well Potential Strange Attractor," *Physica D*, Vol. 17, 1985, pp. 99-108.
14. Craig, R., *Structural Dynamics*, John Wiley and Sons, New York, 1981, pp. 214-217.
15. Dowell, E., "On Asymptotic Approximations to Beam Model Shapes," *Journal of Applied Mechanics*, Vol. 51, June 1984, p. 439.
16. Dugundji, J., "Simple Expressions for Higher Vibration Modes of Uniform Euler Beams," *AIAA Journal*, Vol. 26, No. 8, 1988, pp. 1013-1014.
17. Oden, J., and Ripperger, E., *Mechanics of Elastic Structures*, McGraw-Hill, New York, 1981.
18. Allen, D. and Hailser, W., *Introduction to Aerospace Structural Analysis*, John Wiley and Sons, New York, 1985.
19. Martin, H., and Carey, G., *Introduction to Finite Element Analysis*, McGraw-Hill, New York, 1973.

## INITIAL DISTRUBUTION LIST

- |    |  |   |
|----|--|---|
| 1. | Defense Technical Information Center<br>Cameron Station<br>Alexandria, VA 22304-6145   | 2 |
| 2. | Library, Code 52<br>Naval Postgraduate School<br>Monterey, CA 93943-5002   | 2 |
| 3. | Department Chaiman, Code AA<br>Department of Aeronautics and Astronautics<br>Naval Postgraduate School<br>Monterey, CA 93943-5000              | 1 |
| 4. | Department of Aeronautics and Astronautics<br>ATTN: Professor Ramesh Kolar, Code AA/Kj<br>Naval Postgraduate School<br>Monterey, CA 93943-5000 | 5 |
| 5. | Department of Aeronautics and Astronautics<br>ATTN: Professor I.M. Ross, Code A - /Ro<br>Naval Postgraduate School<br>Monterey, CA 93943-5000  | 1 |
| 6. | Commander M. Sarigul-Klijn, USN<br>965 N. Lincoln St.<br>Dixon, CA 95620   | 1 |
| 7. | Lieutenant Robert G. Vaughan, USN<br>11500 Luxmanor Road<br>Rockville, MD 20852  | 2 |